Technologies to promote neural interface stability

Maran Ma

Integrated Program in Neuroscience
Montreal Neurological Institute
Faculty of Medicine
McGill University
Montreal, Quebec, Canada

December 2020

A thesis submitted to McGill University in partial fulfillment of the requirements of the degree of Doctor of Philosophy in Neuroengineering

Table of Contents

Abstract

Brain-machine-interfaces (BMIs), more broadly, neural interfaces, is a challenging frontier in biomedical engineering because of extensive differences between the nervous system and electronic systems. Neuronal activity is embodied by the flow of ions in an aqueous environment, making the signal difficult to detect. Implanting hardware into neural tissue causes injury to the tissue due to its softness and fragility, and corrosion of the hardware due to its vulnerability to a saline environment. As well, the parallel-processing nature of the brain necessitates recording from a large neuronal population in order to decode a neurological function. Despite these challenges, BMIs may be the most direct avenue to compensate certain disorders of the nervous system. For spinal cord injury for example, even limited use of BMI mediated assistive robotics could have a life changing impact for the patient.

Here we aimed to address three challenges in BMI literature. Clinical recording implants suffer from inconsistent connectivity between neurons and electrodes, which is severely disruptive for the operation of prostheses. Since neurons have been shown to grow synapses onto microbeads coated with synaptogenic polymers, we developed a method to attach bead-like features (micro-pillars) onto any surface, so that neurons may be directed to form hemi-synaptic connections directly onto electrodes enhanced with these features. We tested the response of neurons *in vitro* and observed significant accumulation of synaptic proteins around the micro-pillars, providing evidence that this approach could be effective.

From existing literature, it is unclear to what degree the recording ability of an electrode is compromised by proteins and glial cells that encapsulate the electrode, which typically occurs after implantation. We induced these conditions on an *in vitro* electrode array, performed

electrochemical impedance spectroscopy, and obtained evidence that neither condition affects electrode impedance at 1KHz. We also proposed a circuit representation of extracellular recording that reconciles the role of impedance. The circuit further illustrates that changes to the electrode surface should not have a significant impact on the amplitude of the recorded signal.

The aforementioned instability in the population of neurons recorded by an implant is difficult to measure, thus the state of the art of BMI stability is ambiguous in the literature. Existing approaches to evaluate stability include measuring signal-noise-ratio, which does not reflect the consistency of recorded neurons, and tracking neurons by spike-sorting, which is sensitive to noise and relies on extensive human supervision. We examined a Utah array dataset and found a spike-rate statistic that is related to the relatively unique stimulus-response curve of each neuron. Via this relationship, we formalized a method for stability evaluation that can be reliably automated and built a software tool. We anticipate that the application of this tool may provide the neural interface community an avenue for more standardized stability assessment.

The findings presented in this thesis aim to facilitate the development of enhanced BMIs via technologies that function to bridge the differences between the nervous system and electronic systems.

Resumé

Les interfaces cerveau-machine (ICMs), ou, plus généralement, les interfaces neurales, constituent un défi important en ingénierie biomédicale du fait des différences fondamentales existant entre le système nerveux et les systèmes électroniques. L'activité neuronale est matérialisée par un flux d'ions dans un environnement aqueux, ce qui complexifie la détection du signal. L'implantation d'un matériau électronique provoque des blessures au tissu neural, dues d'une part à la souplesse et à la fragilité du tissu, et d'autre part à la corrosion de l'implant, causée par sa vulnérabilité à un environnement salin. Par ailleurs, le fonctionnement cérébral nécessite le traitement en parallèle d'informations provenant d'une large population de neurones pour décoder une fonction neurologique. Malgré ces défis importants, les ICMs constituent peut-être la piste la plus directe pour compenser certains troubles neurologiques. Dans le cas d'une blessure à la moelle épinière par exemple, l'utilisation, même limitée, d'une assistance robotisée pilotée via une ICM peut avoir un profond impact sur la vie du patient.

Nous ambitionnons ici de répondre à trois problématiques soulevées dans la littérature. Les implants cliniques présentent des défauts de connectivité entre les neurones et les électrodes, ce qui est particulièrement préjudiciable pour le bon fonctionnement des prothèses. Il a été montré que les neurones ont la capacité de produire des synapses à la surface de microbilles recouvertes de polymères synaptogéniques. Nous avons développé une méthode permettant l'arrimage sur n'importe quelle surface de protrusions, dénommées micro-piliers, qui possèdent des caractéristiques similaires à ces microbilles. Des électrodes disposant de telles caractéristiques pourraient ainsi entraîner la formation par les neurones de connections hémisynaptiques. Nous avons testé la réponse de neurones à ce type de dispositif *in vitro*, et avons observé une

accumulation significative de protéines synaptiques autour des micro-piliers, montrant le potentiel d'une telle approche.

Il n'est pas clairement établi dans la littérature à quel point le fonctionnement d'une électrode peut être compromis par les protéines et les cellules gliales qui, typiquement, s'accumulent autour de l'électrode après l'implantation. Nous avons reproduit de telles conditions sur un réseau d'électrodes *in vitro*, et une spectroscopie d'impédance électrochimique nous a permis de montrer qu'aucune de ces conditions ne modifie l'impédance des électrodes à 1 kHz. Nous proposons également une représentation en circuit des enregistrements extracellulaires, permettant de visualiser le rôle de l'impédance au niveau tissulaire. Cette représentation permet également de montrer que les changements à la surface des électrodes n'ont pas d'impact significatif sur l'amplitude du signal enregistré.

L'instabilité susmentionnée de la population de neurones enregistrés par un implant étant difficile à mesurer, l'état de l'art concernant la stabilité des ICMs reste ambigu. Les approches actuelles d'évaluation de la stabilité comprennent d'une part la mesure du rapport signal/bruit, ce qui ne reflète pas la régularité des neurones enregistrés, et d'autre part le suivi des neurones grâce à l'étude des pics de potentiel d'action, qui est sensible au bruit et nécessite une importante supervision humaine. Nous avons étudié une série de données produite en Utah et avons identifié une statistique liée au taux de pics de potentiels d'action associée à la courbe stimulus-réponse relativement unique de chaque neurone. De par cette association, nous avons formalisé une méthode d'évaluation de la stabilité qui peut être automatisée de façon fiable, et avons mis au point un outil logiciel. Nous nous attendons à ce que l'application de cet outil fournisse une piste sérieuse à la communauté travaillant sur les interfaces neuronales pour une meilleure standardisation de l'évaluation de la stabilité des ICMs.

Les conclusions présentées dans cette thèse ont pour but de faciliter le développement d'ICMs optimisés via des technologies permettant de concilier les différences de fonctionnement du système nerveux et des systèmes électroniques.

Acknowledgements

This PhD was a journey in every respect, made possible by too many people to count.

Thank you to my parents, for your unwavering encouragement, objectivity, confidence, and readiness to give me every support you could provide.

Thank you to my supervisor, Dr. Timothy Kennedy, for your trust in my interdisciplinary perspectives, your expertise, and giving me the freedom and support to go as far as I can dream.

Thank you to my co-supervisor, Dr. Bruce Lennox, for your confidence in my potential, inducting me into the Neuroengineering community, and always motivating me to reach higher.

I had the privilege of having a caring and inspiring mentor Dr. Edith Hamel, and dedicated and insightful advisory committee members Dr. Edward Ruthazer and Dr. Vamsy Chodavarapu. Sincere thank you for being there for me as a community of trusted role models.

To collaborators on works beyond my thesis: Jean-Pierre, Jeanne, An, Dominic, Martin, Dr. Hilke, Vincent, Michel, Dr. Lin; your enthusiasm and dedication moved and inspired me.

To my labmates, you are both my teachers and my friends. Thank you for welcoming me to the lab environment at the Neuro and making me feel I belong. Your knowledge and love will always stay with me. Special thanks to Jean-David for translating my thesis abstract.

Thank you to all my personal friends for always believing in me and making me feel at home. Special thanks to Evelyn for keeping me accountable every day as I wrote my thesis, and Henry and Lily for listening with impeccable logic when I was working out ideas.

To people I travelled to conferences with, Camille, Zahraa, and Laila; the times shared with you are highlights in this journey.

Contributions of Authors

Chapter 1 -- Introduction

Maran Ma: Wrote the chapter.

Dr. Timothy Kennedy: Edited the text.

Chapter 2 -- Surface modification with microstructures promote neuronal connectivity with substrate

Maran Ma: Designed and performed biological experiments, developed image analysis program and performed data analysis, assembled figures, wrote the chapter.

Maxime Gagnon: Designed and performed optical microlithography experiments, automated and performed microscopy imaging, provided images for figures 1 bottom A & C, 3 top, and 4 top.

Dr. Santiago Costantino: Assisted Maxime Gagnon with experimental design, assisted with image analysis program and data analysis.

Dr. Timothy Kennedy: Designed experiments and edited the text.

Chapter 3 -- Practical utility of impedance monitoring for neural recording microelectrodes

Maran Ma: Designed and performed experiments, built hardware, performed data analysis, generated all figures, wrote the chapter.

Dr. Mohammadreza Ghavidel: Assisted with protocol.

Dr. Danny Chhin: Edited the text.

Dr. Vamsy Chodavarapu: Provided equipment.

Dr. Janine Mauzeroll: Provided facilities and material.

Dr. Bruce Lennox: Designed experiments.

Dr. Timothy Kennedy: Addressed experimental design and edited the text.

Chapter 4 -- A Standard for Rapid and Reproducible Screening of Neural Interface Stability

Maran Ma: Designed and performed computational experiments, developed software, performed data analysis, generated all figures, wrote the chapter.

Dr. Theodoros Zanos: Designed and performed original *in vivo* recordings, assisted with design of computational experiments.

Dr. Matthew Krause: Designed and performed original *in vivo* recordings.

Dr. Christopher Pack: Designed original *in vivo* studies and edited the text.

Dr. Timothy Kennedy: Designed computational experiments and edited the text.

Chapter 5 -- Discussion & Conclusions

Maran Ma: Wrote the chapter.

Dr. Timothy Kennedy: Edited the text.

List of Figures and Tables

List of Abbreviations

AC: alternating current

AU: arbitrary units (of fluorescence)

BMI: brain machine interface

CNS: central nervous system

DC: direct current

DCC: deleted in colorectal cancer

DCML: dorsal column medial lemniscal

DMEM: Dulbecco's modified Eagle's medium

ECoG: electrocorticography

EEG: electroencephalogram

EIS: electrochemical impedance spectroscopy

FBS: fetal bovine serum

FDA: Food and Drug Administration

FES: functional electrical stimulation.

FPT: firing profile test

HEK: human embryonic kidney

ISI: inter-spike interval

LIF: leaky-integrate-and-fire

MEA: multi-electrode array

NOA61: Norland Optical Adhesive 61

PBS: phosphate buffered saline

PCB: printed circuit board

PDL: poly-D-lysine

PEDOT-PSS: poly(3,4-ethylenedioxythiophene) polystyrene sulfonate

PEG: polyethylene glycol

PNS: peripheral nervous system

PSD95: post-synaptic density 95

PVP: polyvinylpyrrolidone

R&D: research and development

RBR: rule-based reasoning

ROI: region of interest

SCI: spinal cord injury

SFK: Src family kinase

Ti:Sa: titanium-sapphire

USB: universal serial bus

Chapter 1 – Introduction

1.1 Preface

Brain machine interfaces (BMI), and more broadly, neural interfaces, is a frontier in biomedical engineering with tantalizing potential. Clinically, an electronic connection with the nervous system would enable more intuitive control of prosthetic hardware; as well as the possibility of prosthetic software that compensate for disorders within the brain. For the healthy population, depending on implementation, BMI may transform our relationship with technology. In the literature review that follows, we take a brief look at the nature of the interfacing challenge, existing approaches to BMI, and focus on specific areas for further research based on clinical motivation.

1.2 Literature Review

1.2.1 Challenges in brain-machine-interfacing

Given the anticipated benefits of brain-machine-interfaces (BMI) and the innovative capacity of the electronics industry, why does the technology still have critical limitations and low clinical adoption? This section discusses the challenges of BMI, and in particular, how incompatibility between the nervous system and electronic systems exist at many levels.

1.2.1.1 Signal format and location

While both nervous and hardware systems propagate electric signals, they have very little similarity at the device level. Most electronic circuits operate on the flow of electrons through solid state components. “Circuit theory”, upon which circuits are conventionally built and analysed, assumes that *electrical effects happen instantaneously throughout a system* (Nilsson and Riedel 2004). In such idealized *lumped-parameter systems*, components are discrete with concentrated resistance, capacitance, gain, etc. and are interconnected by ideal wires of perfect conductivity. None of the above applies to a neuron, which operates on the flow of ions across semi-permeable membranes arranged in complex continuous structures. And between neurons, signals are typically converted to chemical form. Hence, a precise “equivalent circuit” analysis of even a single unit of neuronal circuitry is non-trivial, because a cell exhibits mixed attributes throughout its body and environment, and signals propagate incrementally via molecular machinery.

Voltages in electronic systems are easily accessible at input/output terminals or at simple wire elements. A neuron in contrast, only exhibits voltages across its cell membrane, which if breached is harmful to the cell. Therefore, long term neural recordings, if performed electrically, must rely on very weak extracellular electric field transients (Blum 2007) that exist in a conductive aqueous environment (Katz 1966), further contributing to measurement difficulty.

1.2.1.2 Hardware substrate and rejection

The massive difference in substrate mechanical properties causes harm to neural tissue when regular electronics are implanted. Similar to the requirement of restoring historic architecture with physically matching – or more pliant – material because motion/expansion differences result in deterioration of the weaker material first (Park 1988), rigid components implanted into soft tissue will injure the surrounding cells during unavoidable displacements from motion or breathing / vascular pulsation (Sridharan et al. 2015; Minev et al. 2015).

Existing recording implants that are used clinically, such as the Utah array, become surrounded by a layer of scar tissue over time, which is exacerbated by the stiffness of the foreign body (Minev et al. 2015; Moshayedi, Ng, and Kwok 2014). Since there is no direct anchoring between target neurons and electrodes, individual neurons fade in and out of the recorded ensemble, with one study finding that only 8% of the initial pool had persisted over 9 months (Vaidya, Dickey, and Best 2014).

The long-term immersion of electrodes in biological fluid also compromises the implant itself. Some investigators suggest hardware breakdown and specifically the deterioration of insulation material are leading causes of signal loss (Prasad et al. 2014; Barrese et al. 2013).

1.2.1.3 Organization and size

The nervous system relies on parallel processing at every level (Kandel, Schwartz, and Jessell 2013), and its pathways are largely "line based", i.e. individual sensory inputs, such as a region of skin, a temperature threshold, occupy a separate axon; similarly, distinct muscles receive signals from distinct fibres in the spinal cord. This is unlike electronic architectures where data can be encoded into 1-2 signals (e.g. USB protocol) to facilitate cabling and connection points. Therefore, to fully interface functionally with a nervous system will require numerous connections. E.g. an ideal artificial eye should conceivably stimulate ~1 million fibers bundled in the optic nerve, which is only ~4 mm in diameter (Jonas et al. 1992).

Processing in the neocortex is argued to be dynamic, distributed, and utilize population encoding. Models suggest that the same neural network outputs can be generated by different internal states, which is supported by the observation that for a given movement, motor cortex population responses exhibit expansive and contractive dynamics that rotate with time (Pandarinath et al. 2015). These characteristics complicate the task of decoding from cortical activity, as the information of interest may be distributed over large/multiple cortical areas and depend on past internal states.

1.2.2 Existing strategies to address challenges

1.2.2.1 Signal format and location

The typical transducer for converting neuronal activity to electronic signals is the electrode. Broadly speaking electrodes exist in two categories: polarisable and non-polarisable / reversible (Blum 2007). In experiments where dissected tissue or cells in culture are probed, it is more effective (or necessary) to enter the cell and measure voltages across the membrane. In this

scenario, reversible electrodes such as AgCl (mediated by intermediary Cl- solution in a pipette) are suitable because currents can directly convert between ions and electrons, and thus not create junction voltages at the electrode interface, which would block DC measurements (Katz 1966).

For long term cell cultures or *in vivo* recordings, where signals must be picked up extracellularly to avoid injuring the cells, polarisable electrodes such as gold or platinum are more suitable. Due to a layer of water molecules (the hydration sheath) that accumulate at the electrode surface, signals are detected indirectly as induced voltages via capacitive coupling. While DC measurements are not possible (which is satisfactory if the signals of interest are mainly action potentials), capacitive coupling gives lower input impedance and thus lower noise, which is beneficial given the extremely small extracellular signal amplitudes. To optimise for low impedance, the electrode-electrolyte coupling could be enhanced for high capacitance, which is a function of surface area. For example, some planar MEA electrodes are made with platinum-black for its rough texture and hence larger equivalent surface area (Blum 2007).

Computationally, simulations using finite-element-models have been employed to better understand and predict factors that affect recorded signals and measured impedances *in vivo*, including the impact of changes at the electrode-electrolyte interface and increased resistivity due to gliosis (Malaga et al. 2015).

1.2.2.2 Hardware substrate and rejection

In attempt to mitigate trauma to cortical tissue, efforts are being made to reduce implant stiffness and volume of tissue displacement. E-Dura (Minev et al. 2015), a soft implant for stimulating and recording in the spinal cord is fabricated from a thin silicone substrate with embedded cracked gold wires and platinum-silicone polymer electrodes. This device maintained

its integrity over 1 million stretching cycles (to 120% original length) and was shown to cause no additional harm than the surgery itself in animal models, while a stiffer implant generated debilitating spinal compression and increased scar tissue. Xie et al. (2015) developed a "macroporous" implant that unfurls microwires out of a wire frame, providing a threefold improvement in sampling efficiency and 20-fold reduction in tissue volume destroyed per electrode when employed as a long term implant.

To improve the integration of implants into the CNS, a myriad of approaches are being investigated (Hofmann and Krüger 2015), including: more flexible/thin implant substrates, coating implants with neural cells encapsulated in soft fibrin hydrogel, and coating implants with conductive polymers enabling anti-inflammatory drug release. Other types of coating, such as PEG, improve the ability for electrodes to avoid protein adsorption, which may affect electrode impedance and contribute to signal quality decline (Sommakia et al. 2014).

Worth noting is a biomimetic strategy that has achieved the best stability to-date. Yang et al. (2019) developed NeuE, an implant consisting of electrodes comparable in size to neuronal cell bodies, linked by a network of extremely thin interconnects (0.9 μm thick by 1 μm wide) that are comparable to the diameter of axons and the flexibility of a myelin sheath. The implant is injected precisely into the brain via a glass capillary. Signal stability was observed on all of 16 electrodes for over 3 months, where the number of neurons recorded per electrode (identified by spike sorting) increased over time and stabilized, and the spike waveforms were remarkably consistent in principle component space. The authors attributed this performance to the physical similarity between the implant and neurons. It would be beneficial to understand exactly why this technology is able to deliver unprecedented stability, to allow engineering of implants that

can be disentangled / removed from the CNS when required, or are otherwise suitable for clinical applications.

An alternative strategy is to avoid invasive contact: the completely non-invasive approach to brain-machine-interfacing is EEG, which is only effective for very large and event driven cortical activity. A promising semi-invasive alternative is ECoG, where electrode pads are placed over the surface of the cortex. Notably, the signals recorded are sufficient to predict object recognition (Miller et al. 2016) and drive individual fingers of a robot prosthesis (Hotson et al. 2016). ECoG however still requires a craniotomy and recent efforts to further reduce invasiveness of neuro-prosthesis have led to ECoG equivalent probes built on stents that can be inserted into cortical veins. This approach would allow ECoG quality signals to be sampled without major surgery for the user, via a catheter angiography (Oxley et al. 2016).

1.2.2.3. Organization and size

Conceptually, the difficulty of the line-based architecture of the brain, the small size of the fibers (~1 μm in diameter), and the self-contained nature of neural tracts can potentially be managed if the pathway of interest connects to a sensory organ. At these biological interfaces, innervation is often spread out into organized, more widely spaced 2-dimenstional arrangements. For example, the cochlear implant, which stimulates the auditory ganglion cells, is positioned on the cochlea where the auditory nerves fan out tonotopically (Guiraud et al. 2007). For patients with retinitis pigmentosa, which degrades photoreceptors of the eye but leaves the optic nerve intact, the state of the art prosthesis, the retinal implant, is seated against the retina where inputs to the optic nerve are distributed geometrically over the fovea (Chuang 2014), giving the user a

low resolution image. In contrast, methods that directly stimulate the optic nerve bundle using a cuff electrode (Veraart et al. 1998) can only induce abstract patterns of phosphenes.

For applications that require connectivity with the cortex, NeuraLink (Musk 2019) has demonstrated a possible strategy of distributing the interface over 96 independent thread like probes. In this system, each thread contains 32 electrode sites, providing a total of 3072 recording channels, with each thread individually inserted by a surgical robot. The robot not only is able to avoid blood vessels, but also serves to precisely implant the interface at locations of interest over a large area (4 cm x 4 cm) on the cortex at high speed. NeuraLink has a significant advantage both in channel count and in spatial coverage compared to traditional arrays bound by a fixed backplane. This platform is complemented by high density electronics that incorporate amplification, digitization, and spike detection within a wireless, fully implanted controller module (Metz 2020; Musk 2019).

Once recorded, signal processing techniques and software design allow for further improvements to the utility of the BMI. Intracortical recordings do not naturally separate individual neurons, as each electrode will pick up all neurons within its recording range and superimpose their activity. For applications (in most cases scientific studies) where neuron identification is required, the technique of spike sorting (Quiroga 2007) theoretically allows data from a single electrode to be decomposed into activity of individual neurons. Due to the spatial arrangement of neurons with respect to the electrode tip, each neuron's action potential will exhibit a slightly different shape, which, together with the inter-spike-interval histograms (Dickey et al. 2009), provides a means to track individual neurons. For decoding algorithms, augmenting the decoding process by taking into account oscillatory wave data, multi-unit recordings, and field potentials, has been shown to produce more consistent BMI performance

(Flint et al. 2013). At the final step, a user interface that continually adapts to signal instability has been demonstrated on a typing prosthesis, which sustained functionality for over a month without explicit retraining (Jarosiewicz 2015).

1.2.3 How to improve BMI functionality

Based on the above, it is unlikely that there will be a "one size fits all" brain-machine-interface for every application. Each implant should be designed according to the biological conditions and specific requirements of the clinical application. One of the most compelling motivations for BMI technology is function restoration for spinal cord injury (SCI). This section discusses relevant background information and potential strategies toward this goal.

1.2.3.1 Spinal cord injury

The spinal cord is comprised of clusters of neuronal cell bodies, local neural circuitry and bundles of axons that send long distance projections. These circuits mediate sensation, muscle activation, and reflex responses. When spinal cord injury occurs, nearby neuronal cell bodies may die, leading to functional loss at nearby spinal segments; at the same time, axonal pathways are interrupted, resulting in paralysis and loss of sensation due to disconnection of all the segments below the injury.

The concept of solving the challenge of spinal cord injury by "reconnecting" across the lesion is not trivial because 1) regeneration in the CNS is very limited due the inhibitory nature of the local environmental and the reduced intrinsic capacity of mature neurons to regenerate, and 2) the ultimate targets of regeneration are far and complex, because the segment of axon that

becomes separated from the cell body cannot survive and the entire length of track requires regeneration, rather than just bridging the gap.

Significant efforts in drug therapy, cell transplantation, and tissue engineering (Kabu et al. 2015) aim to improve the cellular environment at the lesion site and bridge the cavity with scaffolding to facilitate axon re-growth into the lesion and further into the tract beyond the injury site. Perfecting these approaches would be the most natural way to cure SCI and endeavors toward this end are currently work in progress by many laboratories.

1.2.3.2 Neuro-prosthesis approach

A closer look at the organization of CNS motor and sensory pathways provides background on what theoretically needs to be bridged to restore function.

Sensation largely concerns two major spinal cord tracts: the dorsal column medial lemniscal (DCML) pathway, and the anterolateral pathway. DCML conveys proprioception (body position sense) and fine touch sensation. Axons of first order PNS neurons travel directly up the spinal cord and synapse onto the dorsal column nuclei in the brain stem. After SCI, the fibers transected at the lesion location up to the brain stem will degenerate. A hypothetical prosthesis could pick up sensory inputs trapped at the lesion level, and stimulate the target nuclei in the brainstem – this of course raises a major concern of implanting stimulators into a critical collection of cell bodies that gather input from the whole body. The anterolateral pathway has more complex projections, but it would be a lower priority for function restoration as it carries temperature, pain and itch sensation, and lesions on this tract tend to mainly result in loss of pain sensation.

Most voluntary motor movements are activated via the ventral and lateral corticospinal tracts. These tracts contain the downward projecting axons of neurons in the primary and secondary motor areas of the cortex, which at the appropriate spinal segment will synapse onto motor neurons in the ventral horn of the spinal cord. After SCI, the fibers below the lesion location will degenerate. Some quantity of motor neurons populating segments below the lesion level will survive (as the cell bodies are intact in the ventral horn, but lack of stimulation from descending axons will also result in loss of population (Kandel, Schwartz, and Jessell 2013)). A hypothetical prosthesis could pick up activity from axon bulbs that remain at the lesion level, and transmit decoded data to electrical stimulators implanted at lower spinal cord segments.

In current efforts toward functional restoration of quadriplegia, rather than stimulating motor neurons in the spinal cord, which has all the challenges of an interface in the CNS environment, the target muscles or the motor nerves driving the target muscles are stimulated directly via functional electrical stimulation (FES). To this end, cuff electrodes with four circularly positioned electrodes are implanted around the motor nerves (Memberg et al. 2014). The cuff electrodes are engineered to curl to the right tightness and the four sites enable some level of specificity in triggering target fibers. One bottleneck in such a scheme, where a computer can activate upper body movements, is how to best extract motor intent from the user. The most sophisticated FDA approved solution to date is Brain-Gate, a motor cortex implant based on the Utah array device, which unfortunately suffers from poor chronic stability, with as few as 8% of initial neural units persisting after 9 months (Vaidya, Dickey, and Best 2014).

1.2.3.3 Better recordings for prosthesis control

Effective and reliable decoding is a key requirement for a neural prosthesis that controls computing, FES or robotics. If decoding accuracy deteriorates during a task, it will be highly disruptive for the user experience (Jarosiewicz 2015). The duration that a decoder can maintain performance varies significantly, which, depending on implant circumstances, may be as short as 1-2 days (Nuyujukian et al. 2014).

A fundamental issue to consider is why decoders come out of calibration so easily. To elucidate decoder sensitivity, Perge et al. (2013) analysed the within-day changes in single unit data from a Utah array, and found spike rates biased decoded movements in 56% of performance assessments, but only 15% of rate changes can be attributed to movement related recording artefacts, with the remaining 85% likely due to neuron dynamics. Therefore, a major factor in recalibration is volatile cortical dynamics rather than implant performance. However, this issue appears compensable in two ways: motor learning / plasticity, and ensemble decoding. It was found that when decoders are deliberately kept fixed, neural representation will stabilize over time. Monkeys manipulating a cursor via fixed decoders with only 10-15 stable inputs for 19 days eventually gained reliable control (Ganguly and Carmena 2009a). Another study showed that while cursor manipulation grew stable, the system is no better at predicting hand position (Flint et al. 2013). These results indicate that prosthesis specific plasticity can develop within the implant region, but it is task specific and not generalizable to other roles of the local neurons. More promising are reports of circumstances that permitted calibration-free intracortical prostheses, which relied on ensemble decoding (Carmena et al. 2005). One study involving two monkeys with Utah arrays found that when an implant provided over 30 equally contributing channels, the same decoder was effective for two years; while another implant with only a dozen

contributing channels required recalibration every couple of days (Nuyujukian et al. 2014). This finding suggests that if the existing clinical implant technology can simply be enhanced to keep more of its channels active, the user experience may be vastly improved.

Therefore, a more practical question is why the recorded signal declines over time (Barrese et al. 2013). The literature on chronic implant performance points to multiple potential causes (Hofmann and Krüger 2015): electrode impedance changes, chronic glial ensheathment (speculated to insulate the electrode), material failure, and breaking the blood-brain barrier (Prasad et al. 2014). While the latter two factors have clear supporting data, the former two factors are not fully understood or have conflicting evidence, for instance, the observation that a small subset of channels could perform well for years (Vaidya, Dickey, and Best 2014), and that signal amplitudes increase in the first two weeks before leveling off to more or less constant values (Malaga et al. 2015). Malaga et al. (2015) analyzed neural recordings and impedance measurements from chronically implanted Utah arrays, and compared the *in vivo* results with simulation results generated by a FEM model of a Utah array electrode and a NEURON model of a cat layer V pyramidal cell. The authors noted that in the *in vivo* results, while electrode impedance increased over the first three weeks, signal amplitudes increased over only the first two weeks, demonstrating that impedance does not correlate with signal amplitude. And in the simulations, which modeled glial ensheathment with a high resistivity layer between the neuron and implant, results showed that the gliotic tissue does not negatively impact signal amplitude unless it displaces the neurons.

1.2.3.4 New discoveries to leverage

Previous work in the McGill NeuroEngineering group provides important new insight into neuron-substrate adhesion and synaptogenesis, which may enable biological anchoring of neurons onto implants or even precise links between synaptic terminals and electrodes. It was observed that the movement/migration ability of neurons on a surface can be modulated by controlling the ratio of low vs. high affinity coating molecules (PEG and PDL) (Ricoult et al. 2013). More importantly, the neuron's tendency to adhere and form terminal like structures onto poly-lysine coated curved substrates (sub 50 μm beads) (Burry 1980) was studied in detail. Presynaptic specializations formed onto poly-lysine coated microbeads were demonstrated to recycle synaptic vesicles like natural synapses (Lucido et al. 2009), and the hemi-synaptic adhesions formed were found strong enough to pull neurites away using atomic force microscopy (Magdesian et al. 2016). Artificial cell membranes (lipid bilayer with mixed domains) were shown to be similarly synaptogenic when coated on microbeads (Gopalakrishnan et al. 2010). Notably, these lipid coatings are extremely robust and may be embedded with proteins to potentially enhance their synaptogenic capacity. The addition of netrin-1 protein to the bead assay further induced rapid recruitment of both presynaptic and postsynaptic specializations, with extensive local reorganization of F-actin within neurites via DCC and SFK signaling (Goldman et al. 2013). Leveraging the synaptogenic biochemical interactions may ultimately promote the long term stability of such "synthetic synapses".

1.3 Rationale and Objectives

As described in the literature, BMI research is a highly interdisciplinary area with many challenging problems to solve. The studies described in this thesis aimed to contribute to three aspects:

1) Toward enhancing clinical implants to promote stable connectivity with neurons.

We know that clinical MEA technology such as the Utah array suffers from loss of active channels over time, and the inability to record consistently from the same neurons. At the same time, a few arrays have been reported to maintain just enough stable or active channels to support compensatory strategies and allow for reasonable long-term decoding performance. Therefore, it would be beneficial to incrementally enhance either the connectivity with neurons or signal fidelity, without significantly changing the implant design. (This is because each implant design has already been optimized for an application, especially for medical devices in terms of safety.) Results from the synaptogenic microbead assays offer a potential means for such improvements. If an electrode could be modified with features or coatings that promote synaptogenesis onto the electrode, the synaptic adhesion could serve as a physical anchor that keeps the same neurons connected to the same electrodes. Additionally, the physical contact between electrodes and neural processes will improve signal-noise ratio and conceivably allow spikes to be decerned for a longer time period. Thus, the first research objective is to develop a method to modify surfaces with microbead-like features and investigate neuronal response to these surface features.

2) Better understanding of physical phenomena at the electrode-tissue interface and the role of impedance.

We know that after implantation, various physical changes occur to the MEA hardware, neural tissue, and the electrode-tissue interface, all of which may play a role in eventual signal loss. However, it is necessary to understand the degree of impact of each factor in order to inform the best electrode engineering strategies. More specifically, from existing literature it is not clear how exactly biofouling and glial ensheathment negatively affects the neural interface. Impedance measurement, which is currently the most direct means of monitoring electrode and tissue status *in vivo*, is often reported as an indication of stability. Yet its relationship with the recorded signal and the aforementioned physical changes are not clear in the existing literature. Thus, the second research objective is to investigate biofouling and glial ensheathment under controlled conditions (i.e. separately on an *in vitro* platform) in terms of their contributions to impedance changes, and in the process, elucidate what the impedance measure can tell us.

3) Efficient and reproducible methodology for assessment of signal stability.

For a BMI intended to decode and control assistive technology, the true measure of stability would be task performance efficacy over time on a full prosthesis system. Human trials or monkey behavioral studies however, are not suitable for investigators working on the fabrication aspect of the implant technology, which often involve novel materials and interim prototypes. More feasible and prevalent are smaller scale studies that look for some indication of stability in the recorded data, using for instance, rodent models. At the moment, there is a lack of consensus in the community on a stability metric, and a variety of different measures are reported, ranging from physical measures such as signal-noise-ratio, to spike-sorting based

quantities such as “stable unit” count. Although spike-sorting could decern individual neurons, the method relies on waveform shape and is sensitive to noise and implant shift related confounds. Therefore, it often relies on human supervision to ensure accuracy, which hinders the reproducibility and efficiency of the method. Consequently, the stability data on novel neural interfaces is not comparable across different reports, and the state of the art is ambiguous. Thus, the third research objective is to seek patterns in recorded data, without relying on waveform classification, which reflect the stability of the electrode-neuronal connection and formalize this into a stability assessment method.

1.4 References

Barrese, James C., Naveen Rao, Kaivon Paroo, Corey Triebwasser, Carlos Vargas-Irwin, Lachlan Franquemont, and John P. Donoghue. 2013. 'Failure mode analysis of silicon-based intracortical microelectrode arrays in non-human primates', *Journal of Neural Engineering*, 10: 066014.

Blum, Richard A. 2007. "An Electronic System for Extracellular Neural Stimulation and Recording." In. Atlanta: Georgia Institute of Technology.

Burry, Richard W. 1980. 'Formation of apparent presynaptic elements in response to poly-basic compounds', *Brain Research*, 184: 85-98.

Carmena, Jose M., Mikhail A. Lebedev, Craig S. Henriquez, and Miguel A. L. Nicolelis. 2005. 'Stable Ensemble Performance with Single-Neuron Variability during Reaching Movements in Primates', *The Journal of Neuroscience*, 25: 10712-16.

Chuang, A. 2014. 'Retinal implants: a systematic review', *The British Journal of Ophthalmology*, 98.

Dickey, Adam S., Aaron Suminski, Yali Amit, and Nicholas G. Hatsopoulos. 2009. 'Single-Unit Stability Using Chronically Implanted Multielectrode Arrays', *Journal of Neurophysiology*, 102: 1331-39-39.

Flint, R D, Z A Wright, M R Scheid, and M W Slutzky. 2013. 'Long term, stable brain machine interface performance using local field potentials and multiunit spikes', *Journal of Neural Engineering*, 10.

Ganguly, K, and J Carmena. 2009a. 'Emergence of a Stable Cortical Map for Neuroprosthetic Control', *PLoS Biology*, 7.

Goldman, Jennifer S., Mohammed A. Ashour, Margaret H. Magdesian, Nicolas X. Tritsch, Stephanie N. Harris, Nicolas Christofi, Raja Chemali, Yaakov E. Stern, Greta Thompson-Steckel, Pavel Gris, Stephen D. Glasgow, Peter Grutter, Jean-Francois Bouchard, Edward S. Ruthazer, David Stellwagen, and Timothy E. Kennedy. 2013. 'Netrin-1 Promotes Excitatory Synaptogenesis between Cortical Neurons by Initiating Synapse Assembly', *The Journal of Neuroscience*, 33: 17278.

Gopalakrishnan, Gopakumar, Peter Thostrup, Isabelle Rouiller, Anna Lisa Lucido, Wiam Belkaïd, David R. Colman, and R. Bruce Lennox. 2010. 'Lipid Bilayer Membrane-Triggered Presynaptic Vesicle Assembly', *ACS Chemical Neuroscience*, 1: 86-94.

Guiraud, Jeanne, Julien Besle, Laure Arnold, Patrick Boyle, Marie-Hélène Giard, Olivier Bertrand, Arnaud Norena, Eric Truy, and Lionel Collet. 2007. 'Evidence of a Tonotopic Organization of the Auditory Cortex in Cochlear Implant Users', *The Journal of Neuroscience*, 27: 7838.

Hofmann, U, and J Krüger. 2015. 'The chronic challenge—new vistas on long-term multisite contacts to the central nervous system', *Frontiers in Neuroengineering*, 8.

Hotson, Guy, D P McMullen, M S Fifer, M S Johannes, K D Katyal, M P Para, R Armiger, W S Anderson, N V Thakor, B A Wester, and N E Crone. 2016. 'Individual finger control of a modular prosthetic limb using high-density electrocorticography in a human subject', *Journal of Neural Engineering*, 13.

Jarosiewicz, B. 2015. 'Virtual typing by people with tetraplegia using a self-calibrating intracortical brain-computer interface', *Science Translational Medicine*, 7.

Jonas, J B, A M Schmidt, J A Muller-Bergh, U M Schlotzer-Schrehardt, and G O Naumann. 1992. 'Human optic nerve fiber count and optic disc size', *Investigative Ophthalmology & Visual Science*, 33: 2012-18.

Kabu, S, Y Gao, B K Kwon, and V Labhasetwar. 2015. 'Drug delivery, cell-based therapies, and tissue engineering approaches for spinal cord injury', *Journal of Controlled Release*, 219: 141-54.

Kandel, Eric, James Schwartz, and Thomas Jessell. 2013. *Principles of Neural Science 5th Edition* (McGraw-Hill: New York).

Katz, Bernard. 1966. *Nerve, Muscle, and Synapse* (McGraw-Hill: New York).

Lucido, A. L., F. S. Sanchez, P. Thostrup, A. V. Kwiatkowski, S. Leal-Ortiz, G. Gopalakrishnan, D. Liazoghli, W. Belkaid, R. B. Lennox, P. Grutter, C. C. Garner, and D. R. Colman. 2009. 'Rapid Assembly of Functional Presynaptic Boutons Triggered by Adhesive Contacts', *Journal of Neuroscience*, 29: 12449-66.

Magdesian, Margaret H., G. Monserratt Lopez-Ayon, Megumi Mori, Dominic Boudreau, Alexis Goulet-Hanssens, Ricardo Sanz, Yoichi Miyahara, Christopher J. Barrett, Alyson E. Fournier, Yves De Koninck, and Peter Grütter. 2016. 'Rapid Mechanically Controlled Rewiring of Neuronal Circuits', *The Journal of Neuroscience*, 36: 979-87.

Malaga, Karlo A., Karen E. Schroeder, Paras R. Patel, Zachary T. Irwin, David E. Thompson, J. Nicole Bentley, Scott F. Lempka, Cynthia A. Chestek, and Parag G. Patil. 2015. 'Data-driven model comparing the effects of glial scarring and interface interactions on chronic neural recordings in non-human primates', *Journal of Neural Engineering*, 13: 016010.

Memberg, W D, K H Polasek, R L Hart, A M Bryden, K L Kilgore, G A Nemunaitis, H A Hoyen, M W Keith, and R F Kirsch. 2014. 'Implanted neuroprosthesis for restoring arm and hand function in people with high level tetraplegia', *Archives of physical medicine and rehabilitation*, 95: 1201-11.

Metz, Rachel. 2020. 'Elon Musk shows off a working brain implant — in pigs', CNN Business. https://www.cnn.com/2020/08/28/tech/elon-musk-neuralink/index.html.

Miller, K J, G Schalk, D Hermes, J G Ojemann, and R P N Rao. 2016. 'Spontaneous Decoding of the Timing and Content of Human Object Perception from Cortical Surface Recordings Reveals Complementary Information in the Event-Related Potential and Broadband Spectral Change', *PLoS Compulational Biology*, 12.

Minev, Ivan, Pavel Musienko, Arthur Hirsch, and Quentin Barraud. 2015. 'Electronic dura mater for long-term multimodal neural interfaces', *Science Research Reports*, 347: 159.

Moshayedi, Pouria, Gilbert Ng, and Jessica Kwok. 2014. 'The relationship between glial cell mechanose nsitivity and foreign body reactions in the central nervous system', *Biomaterials*, 35: 3919-25.

Musk, Elon. 2019. 'An Integrated Brain-Machine Interface Platform With Thousands of Channels', *J Med Internet Res*, 21: e16194.

Nilsson, James, and Susan Riedel. 2004. *Electric Circuits* (Prentice Hall: New Jersey).

Nuyujukian, Paul, Jonathan C. Kao, Joline M. Fan, Sergey D. Stavisky, Stephen I. Ryu, and Krishna V. Shenoy. 2014. 'Performance sustaining intracortical neural prostheses', *Journal of Neural Engineering*, 11: 066003.

Oxley, T J, N L Opie, S E John, G S Rind, S M Ronayne, T L Wheeler, J W Judy, A J McDonald, A Dornom, T J Lovell, C Steward, D J Garrett, B A Moffat, E H Lui, N Yassi, B C Campbell, Y T Wong, K E Fox, E S Nurse, I E Bennett, S H Bauquier, K A Liyanage, N R van der Nagel, P Perucca, A Ahnood, K P Gill, B Yan, L Churilov, C R

French, P M Desmond, M K Horne, L Kiers, S Prawer, S M Davis, A N Burkitt, P J Mitchell, D B Grayden, C N May, and T J O'Brien. 2016. 'Minimally invasive endovascular stent-electrode array for high-fidelity, chronic recordings of cortical neural activity', *Nature Biotechnology*, 34: 320-27.

Pandarinath, C, V Gilja, C H Blabe, P Nuyujukian, A A Sarma, B L Sorice, E N Eskandar, L R Hochberg, J M Henderson, and K V Shenoy. 2015. 'Neural population dynamics in human motor cortex during movements in people with ALS', *eLife*, 4: e07436.

Park, Sharon. 1988. "The Use of Substitute Materials on Historic Building Exteriors." In.: National Park Service, U.S. Department of the Interior.

Perge, János A., Mark L. Homer, Wasim Q. Malik, Sydney Cash, Emad Eskandar, Gerhard Friehs, John P. Donoghue, and Leigh R. Hochberg. 2013. 'Intra-day signal instabilities affect decoding performance in an intracortical neural interface system', *Journal of Neural Engineering*, 10: 036004.

Prasad, Abhishek, Qing-Shan Xue, Robert Dieme, Viswanath Sankar, Roxanne C. Mayrand, Toshikazu Nishida, Wolfgang J. Streit, and Justin C. Sanchez. 2014. 'Abiotic-biotic characterization of Pt/Ir microelectrode arrays in chronic implants', *Frontiers in Neuroengineering*, 7: 2.

Quiroga, Rodrigo. 2007. "Spike Sorting." In.: Scholarpedia.

Ricoult, Sebastien G, Greta Thompson-Steckel, James P Correia, Timothy E Kennedy, and David Junker. 2013. 'Tuning cell-surface affinity to direct cell specific responses to patterned proteins', *Biomaterials*, 35: 727-36.

Sommakia, S, J Gaire, J L Rickus, and K J Otto. 2014. 'Resistive and reactive changes to the impedance of intracortical microelectrodes can be mitigated with polyethylene glycol under acute in vitro and in vivo settings', *Frontiers in Neuroengineering*, 7.

Sridharan, Arati, Jessica Nguyen, Jeffrey Capadona, and Jit Muthuswamy. 2015. 'Compliant intracortical implants reduce strains and strain rates in brain tissue in vivo', *Journal of Neural Engineering*, 12: 036002.

Vaidya, M, A Dickey, and M Best. 2014. "Ultra-long term stability of single units using chronically implanted multielectrode arrays." In *Engineering in Medicine and Biology Society (EMBC), 36th Annual International Conference of the IEEE*. Chicago.

Veraart, C, C Raftopoulos, J T Mortimer, J Delbeke, D Pins, G Michaux, A Vanlierde, S Parrini, and M C Wanet-Defalque. 1998. 'Visual sensations produced by optic nerve stimulation using an implanted self-sizing spiral cuff electrode', *Brain Research*, 813: 181-86.

Xie, C, J Liu, T M Fu, X Dai, W Zhou, and C M Lieber. 2015. 'Three-dimensional macroporous nanoelectronic networks as minimally invasive brain probes', *Nature Materials*, 14: 1286-92.

Yang, X., T. Zhou, T. J. Zwang, G. Hong, Y. Zhao, R. D. Viveros, T. M. Fu, T. Gao, and C. M. Lieber. 2019. 'Bioinspired neuron-like electronics', *Nat Mater*, 18: 510-17.

Chapter 2 – Surface modification with microstructures promote neuronal connectivity with substrate

2.1 Preface

We begin with the fundamental goal of promoting better connectivity between electrodes and neurons. This chapter is a brief manuscript describing an optical microlithography technique to attach conductive microstructures a substrate, and *in vitro* experiments with cortical neurons to test for biocompatibility and levels of synaptic proteins around the structures.

2.2 Introduction

It is a remarkable phenomenon that a neuron will differentiate a hemi-synaptic specialization onto a poly-lysine coated microbead (Burry 1980, 1982; Peng et al. 1987). Here, we wanted to know if this phenomenon could be leveraged for electrode engineering, and whether it may occur with pillar shaped microstructures attached to a larger substrate.

If this is possible, neural electrodes could then be made with such microstructures that would induce synapse formation directly onto the electrode. Synapses are critical in the central nervous system as they are the point of connectivity between neurons in neuronal networks, and synapses are known to engage strong adhesive connections between pre- and post-synaptic elements. Thus, identifying a way to establish synaptic connection between neurons and electrodes would potentially create a means to 1) anchor neurons onto electrodes, 2) improve signal noise ratio due to close physical contact between a neuron and an electrode, and 3) integrate the electrode into the neuronal network.

Key differences between this investigation and existing synaptogenic bead assays are: 1) the cylindrical microstructure we created are curved along only one axis and will appear different to neurites than a spherical bead, in spite of its curvature; and 2) the microstructures are attached to the substrate and will be a part of the landscape as immature neurites initially extend on the surface. In contrast, beads are typically added to a mature neural culture. We anticipate that the results obtained will increase our understanding of the salient attributes of the substrate that neurons respond to as synaptogenic, and provide practical fabrication methods for electrode engineering.

We devised a technique to polymerize micropillars onto arbitrary substrates by extending the work of Costantino et al. (2005), and tested the response of cultured cortical neurons to these microstructures. We optimized a biocompatible and conductive formula that is compatible with our technique, using a silver nitrate and polyvinylpyrrolidone (PVP) composite (known for its photopolymerization properties (Maruo and Saeki 2008)), and examined synaptogenesis by neurons.

2.3 Results

2.3.1 Polymerization of microstructures

Our engineering objective was to devise a method to build bead like features on an arbitrary surface. The desired features required similar curvature as microbeads used in synaptogenesis assays (5-10 μm diameter), be secure enough that they are not shifted or detached by cells and can be precisely positioned at desired locations on the surface. We initially explored the possibility of adhering existing microbeads with micropatterned surfaces via avidin-biotin binding, but found that cells readily pulled off the beads.

Hence, we investigated using optical microlithography and light curable resins to fabricate microstructures (Figure 1). We optimized a protocol where we coated coverslips with NOA61 resin and focused a two-photon microscope (Ti:Sa laser) at locations of interest to polymerize patterns of dots. Due to the distribution of energy at the focal point, the polymerized zones form short pillars with rounded dome shaped tops. By controlling the laser power and exposure time, it was possible to control the diameter of the pillars. And by automating the microscope stage, arrays of microstructures can be automatically created with precise spatial arrangements. Our final parameters (800 nm laser at 500 mW, 300 ms; with 20x, 0.7 NA objective) produced microstructures with an average height of 6.7±0.8μm and diameter of 5.3±0.3 μm at midpoint. A contributing factor to uncertainties in height was some amount of tilt of the substrate, which affected the quality of focus.

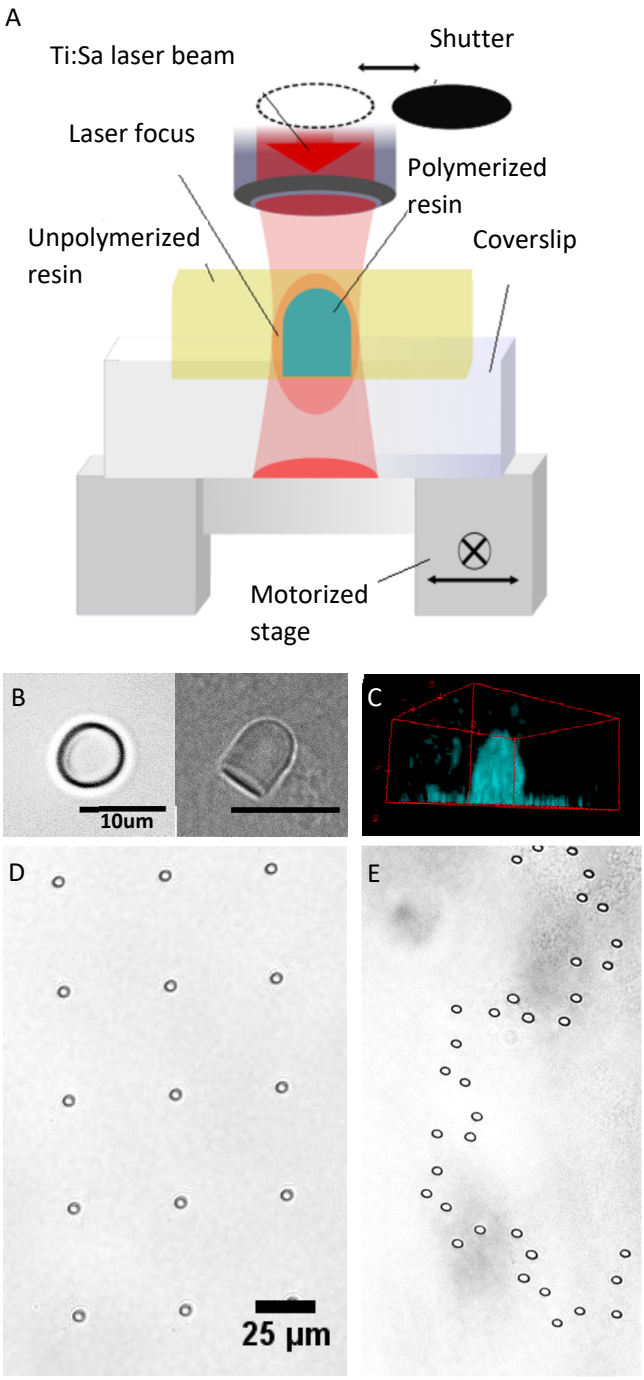

Figure 1. Schematic of the microscope setup to polymerize resin into microstructures on a coverslip (A). A single polymerized microstructure is viewed from the top and on its side in bright field (B), and after one week incubation in cell culture media – rendered from its autofluorescence in confocal images (C). An array of microstructures on a coverslip that is intended for cell culturing (D), and arranged in the shape of a snowflake for demonstration of the technique's ability to precisely control their positions (E).

2.3.2 Assay

For testing with primary neuronal cultures, we optimized the substrate preparation protocol to remove residual unpolymerized resin but not weaken the microstructure's attachment, as well as ensure its sterility. – We found that a brief 100% ethanol wash cleaned the residue and prevented toxicity, but did not result in detached microstructures during immunohistochemistry, and that plasma cleaning was suitable for sterilization.

Traditionally, the analysis of bead experiments involves manual processing of microscopy images: drawing regions of interest (ROI) around tissue contacting beads, and quantifying signal levels relative to nearby tissue not contacting beads. Since our fabrication technique could easily generate thousands of microstructures, it was advantageous to also automate the image analysis process rather than quantify images by hand. We wrote a Matlab application that performed the following (Figure 2): selecting the best focused slice, subtracting cell bodies, subtracting image background using Tubulin immunocytochemistry as a mask, and automatically creating ROIs and control zones at each microstructure. Our strategy was to compare a ring-shaped region, which captures the perimeter of each microstructure, and compare the florescence intensity (indicative of protein accumulation) with an immediately adjacent flat control zone of equal surface area. The center cutout is necessary to minimize including autofluorescence of the polymer in the quantification. We defined a second control zone beside each ROI to monitor that different flat areas have similar intensity. ROI area is calculated using its outer circumference, without subtracting the center cutout. This is because any neurites entering the outer circle must go around the "obstacle" of the microstructure (i.e. are forced to travel the ring-shaped area), and thus for the control zone, neurites that travel anywhere within an equivalent outer circle, including through the center, should be counted.

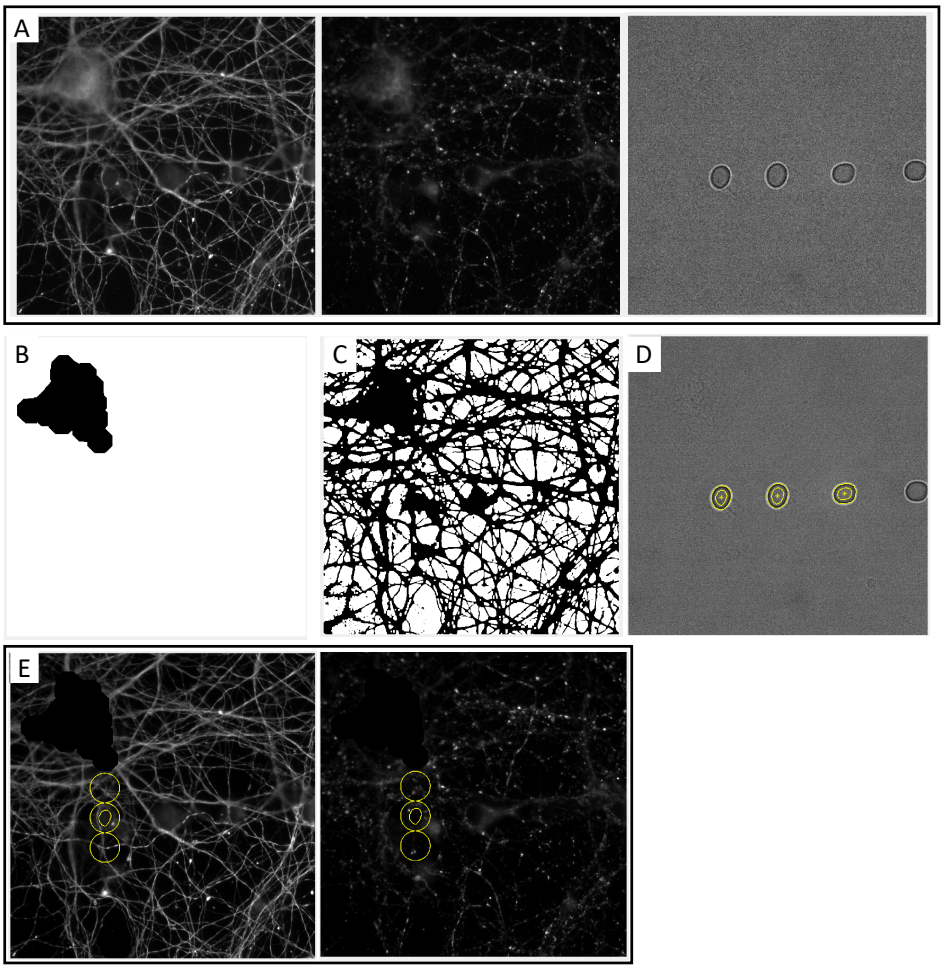

Figure 2. Automated image processing steps. A: selection of best focused slice (shown left to right are fluorescence channels for tubulin, synaptophysin, and a bright-field image for microstructures). B: image mask generated after detection of cell bodies. C: image mask generated after detection of background areas, via segmenting the tubulin channel. D: outlined perimeters of microstructures, after detection of their locations using the bright-field image E: outlined a ring-shaped ROI around one microstructure and two adjacent control zones, after background and cell body subtraction using masks from B & C.

2.3.3 Protein accumulation

As the biological feature of interest is the synapse, we stained samples with two synaptic protein markers (Synaptophysin, found in presynaptic terminals, and PSD95, typically in postsynaptic terminals) as well as a marker for cytoskeleton (Beta III tubulin). Comparing the ring shaped ROI around each microstructure to an adjacent control zone (a flat area of the same size), we found a significant accumulation of tubulin ($p < 0.001$, $n = 246$), synaptophysin ($p = 0.006$, $n = 246$), and PSD95 ($p < 0.001$, $n = 126$) around the microstructures (Figure 3, bottom).

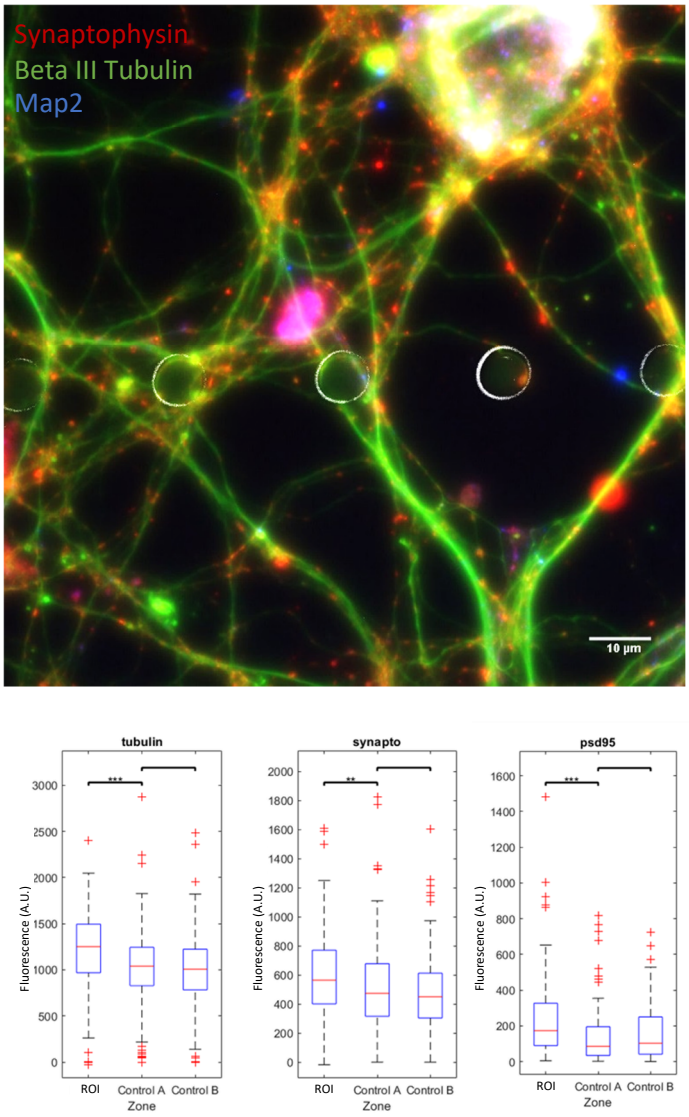

Figure 3. Top: Composite image of neuronal culture and polymer microstructures. Bottom: Comparison of the accumulation of tubulin, synaptophysin, and PSD95 (left to right) around each microstructure vs. an adjacent control zone (***p < 0.001, **p < 0.01), and between two control zones (n.s.). Boxplot box shows median, 25th & 75th percentile; whiskers cover all data points not considered outliers.

2.3.4 Conductive recipe

As the rationale is to modify electrodes, it is important that the microstructures are conductive to augment electrical access to neurons. We tested recipes for a conductive polymer and found that a composite of silver nitrate and PVP can be polymerized using the same optical microlithography setup as the NOA61 resin. We verified that after photoreduction the composite is conductive, at 4E-3 Ωm, and is biocompatible with primary neuronal cultures. During the optimization process, we adjusted the ratio of PVP vs. silver nitrate to balance biocompatibility and conductivity. Too little PVP resulted in reduced neural density within the grid of microstructures, compared to elsewhere on the same coverslip. The final conductive microstructures made had an average height of 4.5±0.6 μm and an average diameter of 8.8±1.6μm at midpoint.

We repeated the cell culture experiment and observed a similar significant synaptic and cytoskeletal protein accumulation associated with the structures (Synaptophysin, $p < 0.001$; PSD90, $p < 0.001$; and Tubulin, $p < 0.001$; Figure 4). The silver-PVP microstructures exhibited more variations in diameter and shape than the transparent polymer, which is due to the non-homogenous distribution of silver in solution. Compared to bulk silver (1.59E-8 Ωm) this composite has lower conductivity due to the presence of residual PVP in the silver matrix.

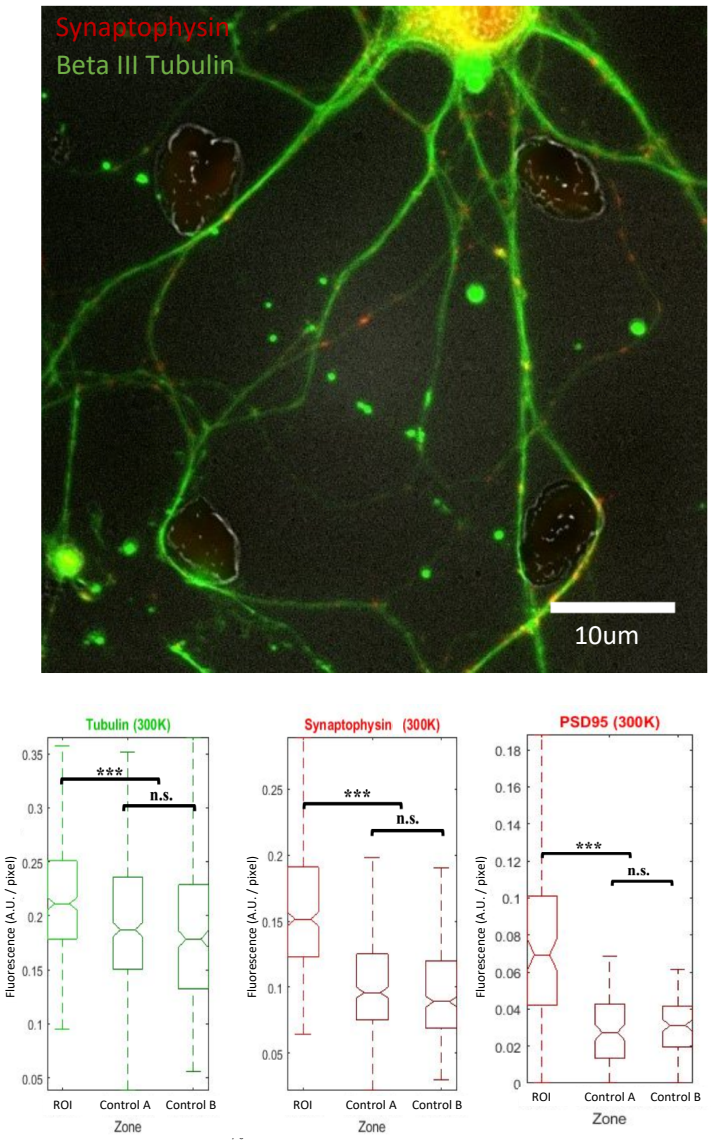

Figure 4. Top: Composite image of neuronal culture and silver-PVP microstructures. Bottom: Comparison of the accumulation of tubulin, synaptophysin, and PSD95 (left to right) around each microstructure vs. an adjacent control zone (***$p < 0.001$), and between two control zones (n.s.). Boxplot box shows median, 25th & 75th percentile; whiskers cover all data points not considered outliers.

2.4 Methods

2.4.1 Fabrication of transparent microstructures

Transparent microstructures were made from UV curing polymer (NOA61) purchased from Norland Inc. The liquid polymer was spread over the substrate by spin coating: first depositing a drop onto a coverslip, attaching it to a rotary tool, then spinning for 15 s at 5000 rpm. Polymerization into desired structures was induced by two-photon absorption using a Ti:Sa laser set to 800 nm directed through a custom built microscope. A 20x objective with 0.70 numeric aperture was used (20x UPlanSApo, Olympus), and precise focused was achieved by observing the laser spot that exits the microscope when the laser is reflected by a glass coverslip exactly at the focal point. Laser power was set to 500 mW, measured after the objective. To automate the process, a mechanical shutter (SH04, Thorlab) was programmed to give exposures of 300ms, and a motorized stage (Thorlab) was programmed to control the position and speed of the laser, both via a custom-made program (LabVIEW 8.1). We fabricated approximately 1000 transparent microstructures using this method.

2.4.2 Fabrication of conductive microstructures

For conductive microstructures, the liquid polymer was made by combining two solutions: 200 mg of polyvinylpyrrolidone (PVP) (average molecular mass 40,000) dissolved in 0.5 mL of 100% ethanol; and 50 mg of silver nitrate ($AgNO_3$) (99.9999% Sigma-Aldrich Co.) dissolved in 0.5 mL of ddH2O. A 200 µL drop of the solution was deposited onto a coverslip and left to dry overnight. The result was a thin transparent layer of yellow to orange colour. Using the same process as described above, conductive microstructures were created by photo-

reduction of the silver nitrate using a Ti:Sa laser. Laser power was set to 17 mW, measured after the objective, and exposure time was set to 500 ms. We fabricated approximately 400 conductive microstructures using this method.

2.4.3 Sample preparation & neuronal culture

Coverslips with microstructures were handled by adding 100% ethanol to the container, and then transferring them inside a TC hood into a sterile 6-well plate. The plate of coverslips was then washed 3 times in sterile ddH2O and aspirated as much as possible, and plasma treated for approximately (no more than) 30 seconds. PDL diluted to 100 µg/mL in HBSS was added (2mL per well) and incubated for 2 hrs at 37°C. The PDL was then aspirated and washed 3 times in sterile ddH2O and left to dry in the TC hood.

Dissociated embryonic cortical neurons from Sprague Dawley rats (E17-E18) were prepared as previously described (Banker and Goslin 1998; Hilgenberg and Smith 2007). Each well was seeded with 200-300K cells with DMEM and 10% FBS and incubated at 37°C. After four hours or overnight, media was replaced with supplemented Neurobasal (Gibco) and incubated at 37°C. After 7 days, half of the media was replaced with fresh supplemented Neurobasal. At 14 days *in vitro*, the cultures were fixed by replacing the medium with ice cold methanol for 8 minutes (at -20°C), then washing 3 times for 5 minutes with 1xPBS, and were stored at 4°C.

2.4.4 Immunohistochemistry

Fixed cultures were blocked and permeabilized with 1xPBS with 5% BSA and 0.25% Triton for 1 hr at rt. The samples were divided into two groups to stain for different synaptic proteins. Group 1 primary antibodies, diluted in blocking solution, consist of anti-PSD95 (rabbit, Cell Signaling D27E11, 1:250 dilution) and anti-Beta 3 Tubulin (mouse, Sigma T8660, 1:250 dilution). Group 2 primary antibodies, diluted in blocking solution, consist of anti-Synaptophysin (mouse, SynapticSystems 101011, 1:500) and anti-Beta 3 Tubulin (rabbit, Abcam AB18207, 1:250 dilution). An additional antibody, anti-MAP2 (chick, GeneTech GTX85455, 1:300) was added to both groups. Samples were incubated with primary antibodies over night at 4°C, and then washed 3 times for 5 min with blocking solution.

Secondary antibodies, also diluted in blocking solution, consisted of goat anti-rabbit (Alexa 488, ThermoFisher A11034, 1:500), goat anti-mouse (Alexa 546, ThermoFisher A11003, 1:250), and goat anti-chick (Alexa 647, ThermoFisher A21449, 1:250). Samples were incubated with secondary antibodies for 1 hr at rt, protected from light. Lastly, samples were washed 2 times for 5 min with 1xPBS and 0.25% Triton, and 2 times for 5 min with 1xPBS. Each sample was quickly submerged in ddH2O and mounted using 5 µL of mounting medium (Prolong Gold) and left to dry at rt (protected from light).

2.4.5 Imaging, image analysis & statistical analysis

Stained samples were imaged using a Zeiss motorized microscope with AxioCam MRm monochrome camera, as a stack of 7 images at different focal planes. Images were automatically processed in Matlab using the following algorithm:

1) Find best focused slice in each stack by comparing the focus score of the Tubulin image using variance of Laplacian method, (Pech-Pacheco et al. 2000; Pertuz, Puig, and Garcia 2013).
2) Detect cell bodies by summing all florescence channels, thresholding and eroding to remove thin neural processes, eroding the inverse image to round out objects, and filtering by size to keep large objects. Keep as cell body mask.
3) Segment Tubulin channel by thresholding and closing the image. Keep as Tubulin mask.
4) Cut out cell bodies by applying the cell-body mask. Subtract background by calculating the mean pixel value of areas not covered by the Tubulin mask, then subtracting it from the entire image (for each channel separately).
5) Detect microstructures, using the brightfield channel, by thresholding and closing the image, then filtering by size to isolate structures. Fill holes and delete any objects touching the edge of the image. Shrink each object to obtain center zones of the microstructure (which should be cut out of the ROI), as well as find their centroids.
6) Create ROIs by creating circle areas around the centroids of each microstructure, then subtracting the uniquely shaped center zones obtained in step 5.
7) Create 2 control zones adjacent to the ROIs. This was decided to be circles of the same outer diameter as the ROI but not removing the cutout. (See Results section for rationale).
8) Tabulate the total of pixel values for each ROI and control zone.

Statistical tests for the effect of the microstructure were performed using an unpaired, two tailed Student's t-test, comparing the ROI and one control zone, another was performed to compare between the two control zones.

2.5 Discussion

From literature, we know that synaptogenesis by neurons can be rapidly triggered using robust artificial substrates, such as beads of a small curvature that are coated with PDL (Lucido et al. 2009). This assay has been expanded and used to investigate different conditions that are sufficient for synaptogenesis (Gopalakrishnan et al. 2010; Goldman et al. 2013). One direction that is yet unexplored is to integrate this knowledge with electrode engineering. The key potential benefit being the possibility of building enhanced stable connections between artificial and neuronal networks. This could provide a vast improvement over a common cause of instability suffered by existing long-term neural electrode implants, which rely on coincidental proximity of electrodes and the neurons recorded.

Thus, we aimed to develop a versatile method of fabrication that could modify commercial electrodes with conductive bead-like features, and test whether a cylindrical curvature could still trigger formation of a hemisynaptic specialization, which would circumvent the challenge of robustly attaching spheres to electrodes.

Our results indicated that optical microlithography can create micron scale pillars with dome shaped tops, of similar dimension as commonly used synaptogenic beads (Lucido et al. 2009; Goldman et al. 2013), precisely onto substrate surfaces. We also found that this technique is effective for silver-PVP composite and optimized a recipe and protocol to fabricate conductive microstructures that are biocompatible with neurons. We observed that such microstructures significantly increased the concentration of pre- and post-synaptic proteins at its edges compared to adjacent flat surfaces of equivalent area. This can be interpreted to mean that given the same

device, such as a brain implant, the addition of microstructures could induce or at least boost the adhesion of both axons and dendrites to the device surface at precisely controllable locations.

Some limitation to these finding include: we only tested the fabrication technique on glass substrates, thus the parameters will need to be adjusted for other materials. Focus is very sensitive for the microstructures to be securely attached, and not all microscopes allow the reflection method of focus testing. Additionally, the precise distribution of synaptic proteins on the microstructures were not tested to confirm if they are true synapses.

Overall, our work offers a practical means to modify commercial electrodes to potentially enable enhanced connectivity with a neuronal network, and brings us one step closer to establishing stable communication with neurons.

2.6 References

Banker, Gary, and Kimberly Goslin. 1998. *Culturing nerve cells* (MIT Press: Cambridge, Mass.).

Burry, Richard W. 1980. 'Formation of apparent presynaptic elements in response to poly-basic compounds', *Brain Research*, 184: 85-98.

Burry, Richard W. 1982. 'Development of apparent presynaptic elements formed in response to polylysine coated surfaces', *Brain Research*, 247: 1-16.

Costantino, S., K. G. Heinze, O. E. Martinez, P. De Koninck, and P. W. Wiseman. 2005. 'Two-photon fluorescent microlithography for live-cell imaging', *Microsc Res Tech*, 68: 272-6.

Goldman, Jennifer S., Mohammed A. Ashour, Margaret H. Magdesian, Nicolas X. Tritsch, Stephanie N. Harris, Nicolas Christofi, Raja Chemali, Yaakov E. Stern, Greta Thompson-Steckel, Pavel Gris, Stephen D. Glasgow, Peter Grutter, Jean-Francois Bouchard, Edward S. Ruthazer, David Stellwagen, and Timothy E. Kennedy. 2013. 'Netrin-1 Promotes Excitatory Synaptogenesis between Cortical Neurons by Initiating Synapse Assembly', *The Journal of Neuroscience*, 33: 17278.

Gopalakrishnan, Gopakumar, Peter Thostrup, Isabelle Rouiller, Anna Lisa Lucido, Wiam Belkaïd, David R. Colman, and R. Bruce Lennox. 2010. 'Lipid Bilayer Membrane-Triggered Presynaptic Vesicle Assembly', *ACS Chemical Neuroscience*, 1: 86-94.

Hilgenberg, L. G., and M. A. Smith. 2007. 'Preparation of dissociated mouse cortical neuron cultures', *J Vis Exp*: 562.

Lucido, A. L., F. S. Sanchez, P. Thostrup, A. V. Kwiatkowski, S. Leal-Ortiz, G. Gopalakrishnan, D. Liazoghli, W. Belkaid, R. B. Lennox, P. Grutter, C. C. Garner, and D. R. Colman. 2009. 'Rapid Assembly of Functional Presynaptic Boutons Triggered by Adhesive Contacts', *Journal of Neuroscience*, 29: 12449-66.

Maruo, Shoji, and Tatsuya Saeki. 2008. 'Femtosecond laser direct writing of metallic microstructures by photoreduction of silver nitrate in a polymer matrix', *Optics Express*, 16: 1174.

Pech-Pacheco, J. L., G. Cristobal, J. Chamorro-Martinez, and J. Fernandez-Valdivia. 2000. "Diatom autofocusing in brightfield microscopy: a comparative study." In *Proceedings 15th International Conference on Pattern Recognition. ICPR-2000*, 314-17 vol.3.

Peng, H. B., D. R. Markey, W. L. Muhlach, and E. D. Pollack. 1987. 'Development of Presynaptic Specializations Induced by Basic Polypeptide-Coated Latex Beads in Spinal-Cord Cultures', *Synapse*, 1: 10-19.

Pertuz, Said, Domenec Puig, and Miguel Angel Garcia. 2013. 'Analysis of focus measure operators for shape-from-focus', *Pattern Recognition*, 46: 1415-32.

Chapter 3 – Practical utility of impedance monitoring for neural recording microelectrodes

3.1 Preface

Next, we delve into physical phenomena at the electrode-tissue interface and the subject of impedance. This chapter is a manuscript describing *in vitro* experiments to precisely characterize impedance changes caused by protein adsorption and a single layer of adhered astrocytes. The manuscript also aims to clarify what the impedance measure represents, its relationship with the recorded neuronal signal, and provide recommendations to improve the utility of impedance monitoring for neural interfaces.

3.2 Introduction

Impedance is a ubiquitous term in the context of recording microelectrodes, but there remains some confusion in its significance and utility. For electrophysiologists accustomed to traditional types of electrodes, such as glass pipettes and tungsten probes, describing electrode impedance is akin to describing electrode tip size (since material conductivity is consistent). -- The physical size of an electrode tip is of course critically important for sensitivity, i.e. the ability to discern signals from individual neurons. In this case, testing electrodes for particularly low impedance values would be helpful for identifying breaches in insulation material.

With the development of optimized materials and surface treatments, such as PEDOT-PSS (poly(3,4-ethylenedioxythiophene) polystyrene sulfonate) and platinum black, it is possible to significantly lower impedance (by means of increased surface texture/area) while maintaining the same electrode footprint. Neto et al. (2018) investigated the performance of low impedance electrodes *in vivo*, by coating half of the electrodes on a polytrode (closely spaced array of ~20 micron pitch) with PEDOT-PSS, and thus the same neuron is recorded by multiple electrodes (some at ~1 MΩ and some ~100 KΩ). The authors found that while there was an improvement in noise (~30%) with low impedance electrodes, there appeared to be no impact on the amplitude of recorded extracellular action potentials.

These examples illustrate that useful understanding/interpretation of impedance values requires knowledge of the underlying cause. For a microelectrode implanted *in vivo*, measured impedance not only depends on electrochemical active area, insulation integrity, but also biofouling, gliosis, and extracellular conductivity. However, it is not uncommon to see reports of

impedance measurements made for chronically implanted microelectrodes and attempts to derive meaning from its trend without adequate strategy to tease apart contributing factors.

A method to thoroughly examine impedance is to make measurements across a wide range of frequencies, via electrochemical impedance spectroscopy (EIS). EIS interrogates a system of interest by applying sinusoidal stimulation signals over a large frequency spectrum (e.g. in our experiment, from 1Hz - 100KHz), and recording voltage vs. current at each frequency, from which magnitude and phase components of impedance can be extracted. Magnitude is the ratio between voltage and current of an AC signal (analogous to conventional resistance), while phase shift is the lag between peaks in current and voltage. Energy storing components such as capacitive cell membranes will cause phase shifts (for example, during depolarization of an action potential, there can be a peak in current flow while the membrane potential is passing through 0V). Using full EIS data, it is possible to derive a model circuit of individual elements that make up an impedance, and if properly fitted, each parameter of each element, including the electrode-electrolyte interface (charge transfer resistance, double layer capacitance), a protein rich layer, glial cells with capacitive cell membranes, and the extracellular space, could all be estimated (Williams et al 2007, Frampton et al 2009). This in theory offers a powerful means to monitor changes in the neural tissue and at the electrode surface.

In practice however, EIS analysis is not readily accessible to complement neural interface applications, due to both the cost of EIS instrumentation and the expertise required to model and fit recorded data.

Thus, this report aims to facilitate practical impedance monitoring for recording microelectrodes. Several aspects are addressed: 1) Clarify the relationship between recorded

neuronal signal, electrode impedance, and impedance measured *in vivo*; by suggesting a simplified circuit representation of the system. 2) Improve understanding of impedance contributions of electrode surface phenomena, such as biofouling and adhered astrocytes, by performing EIS on each condition *in vitro.* 3) Help facilitate accessible impedance monitoring by investigating cost effective EIS hardware and most sensitive test frequencies.

3.3. Results

3.3.1 Impedance in context

As impedance relates voltage and current, it is present in numerous aspects of electrophysiological recording. Most often mentioned are the physical impedance of the electrode prior to contact with tissue, and the impedance measured *in vivo* (typically at 1KHz), which changes over time. From these values, users hope to glean information on surface stability, tissue changes, and implications on the electrode's ability to detect signals, which is often a confusing endeavor. We suggest a simple circuit representation to help reconcile these relationships.

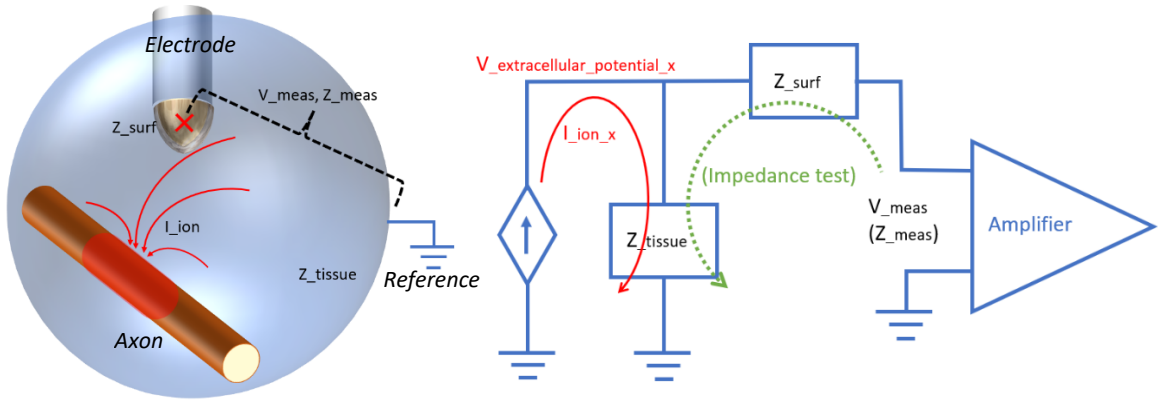

Figure 1. Simplified representation of electrically relevant components of an *in vivo* recording microelectrode. A: An electrode is depicted in the vicinity of an axon that is depolarizing and acting as a current source I_ion. At the electrode tip, intrinsic impedance and surface phenomena make up the impedance Z_surf; beyond the electrode tip, the impedances of neurons, glia, and extracellular matrix constitute Z_tissue; and the recorded voltage or impedance (V_meas & Z_meas) reflect values from the electrode tip (position X) with respect to the reference point, a distance beyond where I_ion is imperceptible. Note that I_ion will travel in all directions and could travel around the electrode (i.e. not be hindered by changes in Z_surf). B: The circuit diagram, in which the recorded voltage is schematized as only dependent on electrode position (I_ion at X) and tissue impedance, while the recorded impedance includes tissue, electrode, and surface phenomena.

As an action potential propagates through a neuron, the large membrane potential spike is mediated by ionic current flow across the cell membrane at that location on the cell. The exact

transmembrane current is determined by the mechanisms that underlie the generation of the action potential and the cell membrane properties, and thus is considered a fixed current source. The current then dissipates via volume conduction into the aqueous environment. A certain distance away, shown as a sphere in Figure 1A, the current is almost imperceptible; this will be considered equivalent to "ground". We can detect the action potential if a recording microelectrode is placed within the volume where the current is dissipating (ideally as close as possible to the current source), and a reference electrode outside of it.

The resulting extracellular potential (i.e. signal of interest) near a neuron is a function of the ionic current at that point in space and extracellular conductivity (Pettersen et al. 2012). Consider, as ionic current from the neuron travels in all directions that lead to "ground", the current will favour paths of least resistance, and thus the presence (and intrinsic impedances) of an electrode nearby will have negligible impact on the net path to ground perceived by the current source. With this premise, we represented the ionic current at the electrode's location as a current source that is a function of distance to the neuron, and represented the extracellular conductivity and the electrode related impedance as parallel paths to ground (Figure 1B). The extracellular potential is labeled to emphasize that the voltage signal we record is primarily determined by electrode's distance to the neuron and tissue impedance (assuming of course the electrode tip is sufficiently small). And the electrode impedance as well as interface phenomena could thus be considered a part of the recording equipment.

In this circuit representation, the electrode and its surface related impedances (lumped into Z_{surf}) is in series with the extracellular potential and the recording amplifier. Therefore, Z_{surf} only poses a problem if a significant voltage divider is formed with the amplifier's internal resistance (as mentioned by Neto et al. (2018)).

The circuit also illustrates that when impedance is measured *in vivo*, the result incorporates both Z_{surf} and tissue impedance (Z_{tissue}, which includes the extracellular matrix, other neurons, and glia). As described above, Z_{surf} has a negligible impact on signal amplitude, while Z_{tissue} plays a significant role. Z_{tissue} is also a function of tissue composition, where glial scars are more dense than typical healthy neural tissue and has higher impedance (Williams et al. 2007).

We suggest that based on this circuit representation, it is reasonable to investigate and interpret gliosis progression using impedance measurements *in vivo*. Since measured impedance is the sum of Z_{tissue} and Z_{surf}, then Z_{tissue} can be estimated by subtracting Z_{surf} from the measured impedance. Z_{surf} in turn consists of an electrode's intrinsic impedance and effects of surface phenomena. Intrinsic impedance can be measured before implantation (if not provided by the manufacturer), and material changes can be stress tested separately (Xie et al. 2014). In subsequent results we show EIS data for common surface phenomena (i.e. biofouling and a single layer of adhered astrocytes), which can serve as a reference for the contribution of these elements to Z_{surf}.

3.3.2 Characterization of electrode surface changes

To understand the contributions of surface phenomena in the cumulative impedance of implanted electrodes, we tested common surface conditions using an *in vitro* array designed for neural electrophysiology (AxionBioSystems, M64-GL1-30Au200). The MEA pads were gold (30 μm diameter, 200 μm spacing), with traces insulated by 5 μm thick SU8, on a glass substrate, integrated into a cell culture well. We built a custom adapter with a 3D printed socket to seat and

connect to the MEA well. Via the adapter, it was possible to freely access the 64 microelectrode pads and 4 large ground pads of the device.

We performed EIS using a multi-potentiostat (Bio-Logic VSP-300) in 3-input configuration: the working input was connected to an electrode of interest; the counter input was connected to the 4 ground pads (to source/sink current for the working input); and the reference input was connected to a silver/silver chloride (Ag/AgCl) wire that was dipped into the MEA well. The reference wire was verified against a mercury sulphate standard before each recording session.

Biofouling

The biofouling condition was created by incubating the MEA in 100% fetal bovine serum (FBS), and measured using on day 0 (before incubation), after 2 days, and after 5 days. The measurements were made across a frequency range of 1Hz - 100KHz on 10 gold microelectrode sites in DMEM solution. We observed that at 1KHz, the central frequency for action potentials, impedance was unaffected, both in magnitude and phase shift (raw data in Figure 2A, t-test results in Table 1).

Adhered cells and PDL coating

The surface glial encapsulation condition -- a single layer of adhered cells, was created by culturing astrocytes on a PDL coated MEA. Measurements were made on 12 gold microelectrode sites in PBS solution: on a new MEA, after PDL coating, and after 2 days of astrocyte growth. We observed that at 1KHz, impedance magnitude was not affected by either PDL coating or the astrocytes, but that the phase shift was more negative (i.e. surface is more capacitive) after PDL coating (raw data in Figure 2B, t-test results in Table 1).

3.3.3 Frequencies of interest

From the raw EIS data (Figure 2), it is apparent that lower and higher ends of the measured frequency spectrum are more sensitive to surface changes, while 1KHz, the most often reported measure in literature, was the least affected. We performed paired t-tests with Bonferroni-adjustment at frequency points closest to each order of magnitude (Table 1). Indeed, for the 30μm diameter gold microelectrodes we used there was no significant magnitude difference due to any of the tested surface changes at 1KHz.

This result makes the 1KHz *in vivo* impedance uniquely useful for similar microelectrodes, and suggests that there are frequencies where observed impedance changes mostly reflect changes in tissue composition beyond the immediate surface of the electrode. This, of course, assumes that the electrode's intrinsic impedance is stable, which could be stress tested without implanting *in vivo* (Xie et al. 2014). At the same time, if electrode surface phenomena are of interest, single frequency impedance testing should be performed at more sensitive frequencies. Our observations indicated that the phase data at 10KHz and at very low frequencies (10Hz or below) are the most effective at detecting surface changes.

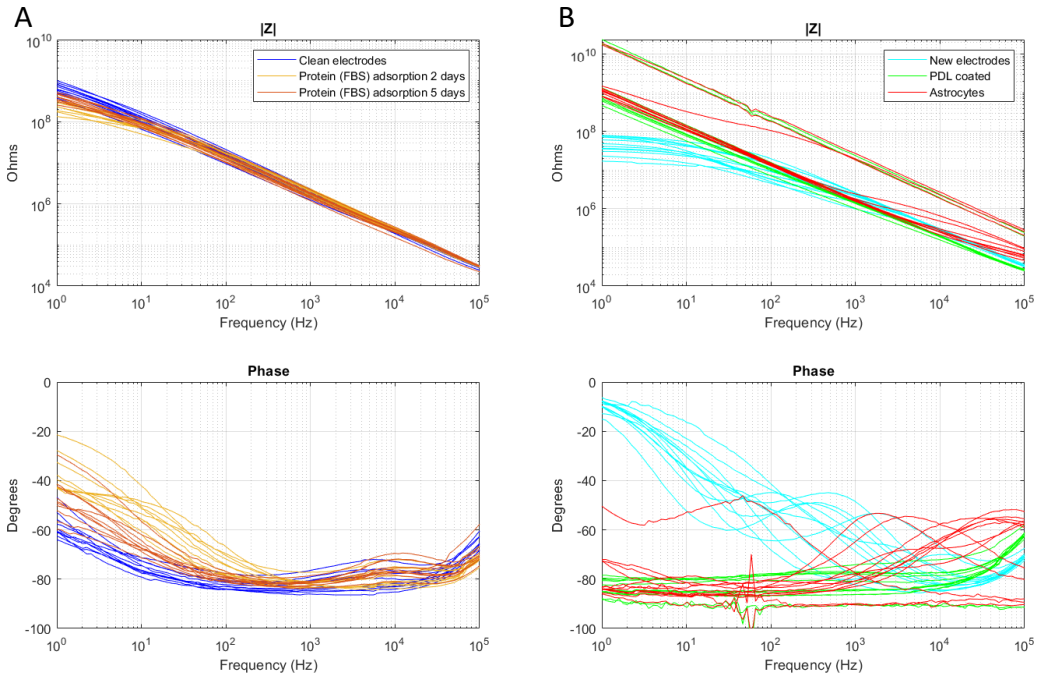

Figure 2. Raw EIS data presented in Bode plot format, where impedance magnitude and phase shift components are plotted separately over the range of stimulation frequencies. A: biofouling experiment, recorded on 10 microelectrodes on bare (cleaned) electrodes, after 2 days, and 5 days of protein adsorption. B: astrocyte experiment, recorded on 12 microelectrodes on bare (new) electrodes, after PDL coating, and after culturing a layer of astrocytes, .

Table 1. Impedance differences tested at 6 frequencies assessed using paired Student's t-test. Significant differences are shown as the mean change in impedance (average of 10 or 12 electrodes), followed by Bonferroni adjusted p-values.

Frequency:	**1.0Hz**	**10.2Hz**	**105Hz**	**1.07KHz**	**11.0KHz**	**100KHz**
Impedance Magnitude						
New vs. PDL coated						
PDL vs. astrocytes						+54KΩ p=0.017
Clean vs. 2-day biofouling	-440MΩ p<0.001	-39MΩ p=0.036				
2-day vs. 5-day biofouling	+149MΩ P<0.01					
Impedance Phase shift						
New vs. PDL coated	-74° p<0.001	-52° p<0.001	-30° p<0.001	-16° p=0.013		
PDL vs. astrocytes					+11° p=0.015	
Clean vs. 2-day biofouling	+21° p<0.001	+22° p<0.001	+8° P<0.01		+1° p<0.001	-6° p<0.001
2-day vs. 5-day biofouling	-10° p<0.001	-13° p<0.001	-5° p=0.013		+3° p<0.001	

3.3.4 Cost effective EIS

Accurate EIS instrumentation is generally prohibitively expensive for many non-specialist research laboratories; for this reason, prior to recording with the multi-potentiostat we briefly explored a cost-effective alternative: the AD5933 12-bit impedance converter chip from Analog Devices. AD5933 is available on a ready-to-use evaluation board (EVAL-AD5933EBZ) with USB connectivity and software interface. This technology offers a unique opportunity for EIS to be portable and extremely affordable (at ~$60 USD).

Although the recorded data we obtained are not of sufficient accuracy for impedance research, some results are summarized here. The accessibility of this technology may allow impedance monitoring that complement neural interfaces to be one step more sophisticated than the single-frequency magnitude-only data found in literature.

The EVAL-AD5933EBZ board by default employs a 16 MHz oscillator. We replaced the oscillator with a 4MHz component in order to record in the 1KHz-10KHz range. The rest of the setup consists of the same MEA and custom adapter as described above. As AD5933 only supports two input mode (where the second input serves as both reference and counter), we used the large ground pads of the MEA for the second input. Although gold pads do not serve as a good reference, it would be more stable than an Ag/AgCl wire when a current is driven across it.

Surface conditions tested include PDL coating and growing HEK293 cells (Shaw et al. 2002), a cell line derived from human embryonic kidney cells, at two confluence levels. The PDL coating was detected with statistical significance at 10KHz in phase shift. Other differences can be seen in the averaged impedance plots (Figure 3A) but were not significant, likely due to the low number of electrodes tested (4 electrodes). Comparatively, the measurements derived

from two different MEA plates under identical conditions appear very closely matched (Figure 3B). These findings support the precision of AD5933 as a tool to detect relative impedance changes. However, a key drawback is reflected in Figure 3C (upper graph): it is necessary to preset the device with the anticipated range of the impedance under test. Due to the hardware design, impedances beyond the upper end of the preset range will be affected by artefacts while impedances beyond the lower end will be clipped. Therefore, another method of impedance measurement is still needed to support the AD5933, but at its price point, the findings obtained indicate that this is a valuable tool for gathering qualitative impedance insights.

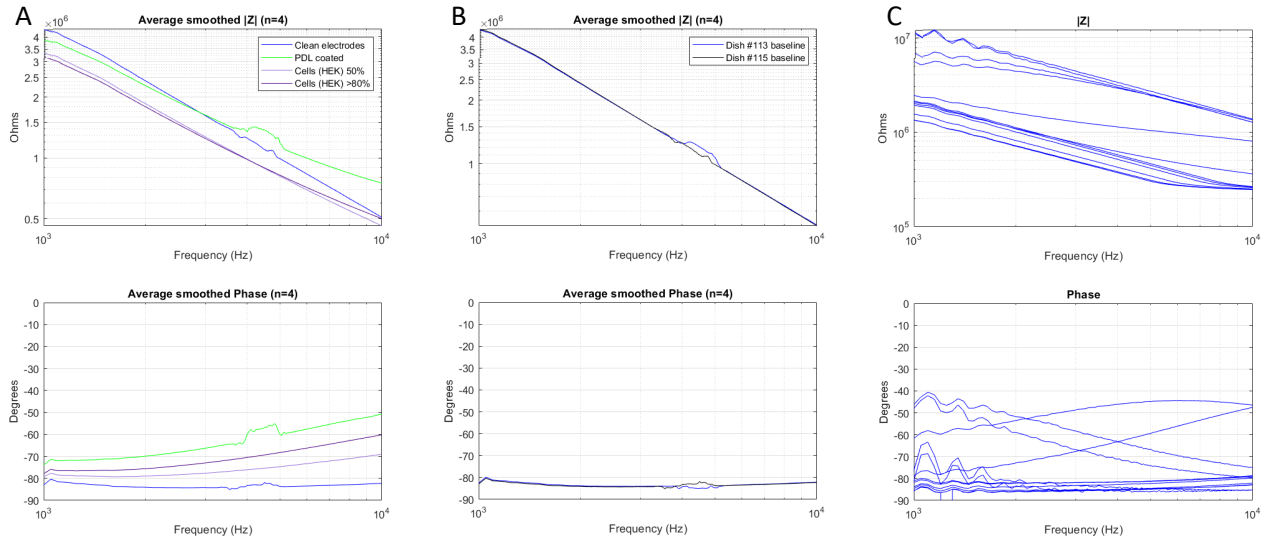

Figure 3. EIS data recorded using AD5933 impedance converter: PDL coating and HEK cell culture conditions (A), and baseline condition from two MEA plates (B). Each condition was averaged over 4 recorded microelectrodes and smoothed to reduce artefact and noise. Example of raw data (C) illustrates artefacts and clipping at the upper and lower end of calibrated range respectively.

3.4 Methods

3.4.1 MEA adapter board

A custom printed circuit board (PCB) was made to gain access to output pins of the MEA (AxionBioSystems, M64-GL1-30Au200). The MEA's 64 electrodes (in an 8x8 matrix) are connected out from the glass substrate to pads on a small circuit board at the base of the MEA plate in a non-standard layout. The base of the MEA was first photographed on a scanner in order to measure the dimensions and positions of the output pads. The custom PCB was laid out with pads of identical footprint as the MEA, which were then connected out to a large matrix of plugs. The plugs were arranged such that the position of each plug matched the position of its connected electrode inside the MEA. (This is so that if an electrode of interest is observed under the microscope it will be easy to find its plug.)

To enable electrical connectivity between the MEA and the PCB, a custom socket was made via 3D printing and mounted onto the PCB. The socket has two elements, an outer element that the MEA plate securely seats into, and an inner element that holds 4 pieces of Z-axis elastomer (Z-Axis Connector Company). Z-axis elastomer is a material that is an insulator in 2 (X and Y) dimensions but a conductor in the 3rd (Z) dimension when it is compressed in this dimension. Therefore, the material allows two devices with matching footprints to be electrically connected when the elastomer is sandwiched between them.

3.4.2 Biofouling and PDL coating

The biofouling condition was created with heat inactivated fetal bovine serum (FBS). The FBS was sterilized by filtering, added to a cleaned (previously used) MEA at 100%

concentration, and incubated at 37°C. Before an EIS measurement, the FBS was slowly poured out, the MEA well was then gently filled with medium so as to not disturb the adsorbed layer of protein.

A new MEA was prepared for the astrocyte culture condition. The MEA was first sterilized with 70% ethanol for 5 min, washed 3 times in ddH2O, dried with a vacuum, and then plasma treated for 30 sec. The sterile MEA was then coated with PDL, which is necessary for cell adhesion. PDL was first diluted to 100 µg/mL in HBSS, filtered, then added to the MEA and incubated for 2 hrs at 37°C. The solution was then aspirated and the MEA washed 3 times in sterile ddH2O and left to dry in the TC hood.

3.4.3 Astrocyte culture

Astrocytes were obtained from a P1 postnatal rat glia culture, after a shake off procedure that is used to harvest oligodendrocytes, leaving behind astrocytes and some microglia in the culture flask (Armstrong 1998). The flask was first filled with 1X trypsin-EDTA and incubated for 2 min to detach the cells. The mixture was spun down, resuspended in DMEM and passed through a cell strainer. The resuspended cells were counted and ~ 0.25 million seeded on the MEA, in DMEM with 10% FBS, and incubated at 37°C.

3.4.4 EIS recording on multi-potentiostat

EIS recordings were made using the multi-potentiostat (Bio-Logic VSP-300) with a high sensitivity probe, controlled through its software interface (EC-Lab V10.44). The MEA was

seated into the custom adapter described above, which along with the probe was placed inside a grounded faraday cage.

The potentiostat was configured to make 3-input recordings. The working input was connected to electrode(s) of interest on the MEA, manually connected one at a time. The counter input, which serves to source/sink currents for the working input, was connected to the four large ground pads of the MEA, which were linked together with wires on the adapter board. The reference input was connected to an Ag/AgCl wire that was dipped into the MEA well. The reference wire was prepared by soaking a silver wire in bleach, and stored in saturated KCl.

Before each recording session, the reference wire was tested against a mercury sulphate standard electrode. Before recording from each electrode, a constant voltage of 50 mV was driven for 5 min in CA mode in order to stabilize transient surface effects. Recordings were then made in PEIS - floating mode, sweeping from 1Hz to 100KHz over 100 logarithmically space points, with a stimulation signal at 50 mV offset (Frampton et al 2009) and 10 mV amplitude.

3.5 Discussion

Impedance is often a point of discussion relating to neural recording electrodes. Generally, people are interested to know if an electrode design is suitable for an application, and for long term implants, to track how the implant and surrounding brain tissue is faring over time, for which impedance testing is the only way to interrogate the system *in vivo*.

Long term reliability of neural implants is itself an active and challenging area of research. Loss of signal may be attributed to a number of factors, including insulation break down, biofouling, gliosis, and neuronal death (Prasad et al. 2014). To build the most stable interface, it is important to know which factors contribute most to the decline of recorded activity and select engineering strategies accordingly. Since impedance measured *in vivo* is a function of most of these factors, it could provide valuable insights for improving electrode design.

Given the all encompassing nature of impedance however, it can be difficult to interpret the data and understand its significance. Taking intrinsic impedance as a specific example, while classical electrophysiologists consider a high value a positive indication, this is valid only when the quantity reflects electrode size. Neto et al. (2018) showed that given the same electrode size, impedance differences due to material/texture do not affect signal amplitude.

The technique of electrochemical impedance spectroscopy potentially allows investigators to harness the full power of impedance monitoring for neural implants. The raw data, by inspection, could reveal signs of extensive reactive gliosis (Williams et al. 2007), and an equivalent circuit could further be derived and fitted to provide estimates of each physical and biological element (Frampton et al. 2009). These techniques however are not generally

accessible outside of dedicated impedance research due to equipment cost and expertise required for modelling.

Our report aimed to shed light on the information provided by impedance measurements in the context of neural recording electrodes, and how to monitor it more effectively for different purposes.

To this end, we suggested a simple circuit representation of the electrically relevant elements of a recording implant. This representation relies on the mathematical model of the origin of extracellular spikes (Pettersen et al. 2012) and delineates which elements contribute to the measured action potential vs. the measured impedance. It was simplified as much as possible to facilitate an intuitive view.

The circuit model shows that 1) the amplitude of the measured action potential mainly depends on tissue impedance and ionic current that is a function of the distance to the neuron. 2) The electrode/surface impedance is in series with the headstage amplifier and can be considered a part of the recording equipment. 3) The measured *in vivo* impedance incorporates all these impedances. This could fit and reconcile relevant findings in literature. For instance, simulation results presented by Malaga et al. (2015) indicate that effects at the interface such as biofouling and glial encapsulation should not negatively affect recorded signal amplitude, but increased distance to the neurons due to displacement by scar tissue would significantly reduce signal amplitude. As mentioned above, Neto et al. (2018) provide evidence that intrinsic electrode impedance does not affect signal amplitude, but the voltage divider with the amplifier may become an issue. And the fact that impedance measured *in vivo* seems to consistently follow a time course related to healing and scar development (Barrese et al. 2013; Malaga et al. 2015), but does not have a simple correlation with action potential amplitude, could plausibly be due to

gliosis both increasing tissue resistance in the neighbourhood of recorded neurons, but also increasing the distance to these neurons.

The circuit also implies that tissue impedance can be estimated if the electrode and surface related impedances (Z_{surf}) is accounted for. This is feasible by characterizing surface phenomena in a controlled environment. We performed EIS for the surface conditions of biofouling and a single layer of adhered astrocytes, and found that different frequencies have different sensitivity to these conditions. Therefore, at a frequency where surface changes are "invisible", changes in tissue impedance, which can reflect gliosis progression, could be observed directly.

Here, we also briefly tested an affordable EIS tool, the AD5933 impedance converter, and found it has promising precision/sensitivity, but is encumbered by the requirement for calibration.

In summary, we recommend the following practices to improve the utility of impedance monitoring: 1) Augmenting measurements to complex impedance at 3 frequency points (e.g. 10Hz, 1KHz, and 10KHz), with baselines taken before and after implantation. 2) For novel electrode materials, observing if its impedance has a stable profile over time (e.g. in PBS at physiological temperatures) to account for this variable. 3) A few rules of thumb for data interpretation -- at 1KHz, values above the post-implant baseline likely reflect tissue reactivity, values below likely reflect compromised insulation; and to look for phase shifts at 10KHz/10Hz to detect changes at the electrode surface.

3.6 References

Armstrong, Regina C. 1998. 'Isolation and Characterization of Immature Oligodendrocyte Lineage Cells', *Methods*, 16: 282-92.

Barrese, James C., Naveen Rao, Kaivon Paroo, Corey Triebwasser, Carlos Vargas-Irwin, Lachlan Franquemont, and John P. Donoghue. 2013. 'Failure mode analysis of silicon-based intracortical microelectrode arrays in non-human primates', *Journal of Neural Engineering*, 10: 066014.

Frampton, John P, Mathew R. Hynd, Aytekin Vargun, Badri Roysam, and William G. Shain. 2009. 'An in vitro system for modeling brain reactive responses and changes in neuroprosthetic device impedance', *2009 Annual International Conference of the IEEE Engineering in Medicine and Biology Society*: 7155-58.

Malaga, Karlo A., Karen E. Schroeder, Paras R. Patel, Zachary T. Irwin, David E. Thompson, J. Nicole Bentley, Scott F. Lempka, Cynthia A. Chestek, and Parag G. Patil. 2015. 'Data-driven model comparing the effects of glial scarring and interface interactions on chronic neural recordings in non-human primates', *Journal of Neural Engineering*, 13: 016010.

Neto, Joana P., Pedro Baião, Gonçalo Lopes, João Frazão, Joana Nogueira, Elvira Fortunato, Pedro Barquinha, and Adam R. Kampff. 2018. 'Does Impedance Matter When Recording Spikes With Polytrodes?', *Frontiers in Neuroscience*, 12.

Pettersen, Klas H., Henrik Linden, Anders M. Dales, and Gaute T. Einevoll. 2012. 'Extracellular spikes and current-source density.' in Romain Brette and Alain Destexhe (eds.), *Handbook of Neural Activity Measurement* (Cambridge University Press).

Prasad, Abhishek, Qing-Shan Xue, Robert Dieme, Viswanath Sankar, Roxanne C. Mayrand, Toshikazu Nishida, Wolfgang J. Streit, and Justin C. Sanchez. 2014. 'Abiotic-biotic characterization of Pt/Ir microelectrode arrays in chronic implants', *Frontiers in Neuroengineering*, 7: 2.

Shaw, Gerry, Silas Morse, Miguel Ararat, and Frank L. Graham. 2002. 'Preferential transformation of human neuronal cells by human adenoviruses and the origin of HEK 293 cells', *FASEB journal : official publication of the Federation of American Societies for Experimental Biology*, 16: 869-71.

Williams, Justin C., Joseph A. Hippensteel, John Dilgen, William Shain, and Daryl R. Kipke. 2007. 'Complex impedance spectroscopy for monitoring tissue responses to inserted neural implants', *Journal of Neural Engineering*, 4: 410.

Xie, X., L. Rieth, L. Williams, S. Negi, R. Bhandari, R. Caldwell, R. Sharma, P. Tathireddy, and F. Solzbacher. 2014. 'Long-term reliability of Al2O3 and Parylene C bilayer encapsulated Utah electrode array based neural interfaces for chronic implantation', *J Neural Eng*, 11: 026016.

Chapter 4 – A standard for rapid and reproducible screening of neural interface stability

4.1 Preface

Lastly, we work with the recorded signal to address a gap in the available tools for stability assessment. This chapter is a manuscript advocating a method and software, the Firing Profile Test (FPT), for systematically detecting changes in firing patterns related to changes in the recorded neuronal population. Also included in the report are an estimate of FPT accuracy determined by simulated ground-truth data, a comparison against spike-sorting based methods, and stability results from applying FPT to two long-term Utah array datasets.

4.2 Abstract

Neural interface technologies, such as microelectrode-arrays, provide high-fidelity recordings of neuronal activity for neurological research and to drive prosthetic devices, yet, widespread clinical adoption is hindered by unstable connections between neurons and recording sites. Developers and users lack effective and reproducible methods for stability assessment. Current approaches are labour intensive and prone to bias that confounds reproducibility, limiting the capacity to interpret neural interface data and constraining progress in the field. To address this, we developed the Firing Profile Test (FPT), a fully automated stability evaluation method that analyzes spike rate attributes to detect changes in a neural population. We demonstrate that FPT delivers comprehensive stability profiles of microelectrode-arrays, to provide high-speed reproducible stability assessment that will facilitate neural interface R&D, enhance the utility of existing interfaces, and enable the development of neural decoders that adapt to instability.

4.3 Introduction

Microelectrodes are employed in brain-machine-interfaces (BMI) for neuroprostheses and electrophysiology studies to capture spiking activity of individual neurons. Array devices with up to hundreds of channels (electrode sites) are available as implants for the central nervous system (CNS) or peripheral nervous system (PNS) (Hochberg et al. 2012; Normann and Fernandez 2016). Long-lasting microelectrode implants that deliver stable recordings are necessary for practical prostheses and for tracking neural correlates of behavior, learning and plasticity. However, achieving stable neural-implants is particularly challenging, due to factors such as the small size of the signal source and amplitude, hardware deterioration and fouling, softness and fragility of neural tissue, and the foreign body response (Salatino et al. 2017; Barrese et al. 2013; Prasad et al. 2014). Consequently, a significant volume of research is directed toward developing more biocompatible and robust implants (Rivnay et al. 2017; Bettinger 2018).

Essential to innovation is performance assessment. Without precise and timely testing of a novel design, another R&D iteration cannot proceed due to the lack of clear targets for improvement and the loss of expertise and momentum. Equally important is reproducibility. If a test relies on human decisions, reports from different groups are not directly comparable, hence, the literature becomes ineffective at elucidating the state of the art for user adoption and for groups advancing the state of the art to compare and evaluate progress.

Lacking consensus on evaluation criteria (Durand, Ghovanloo, and Krames 2014), the neural interface community currently employs a variety of stability evaluation methods (summarized in Table 1). The likely cause of this disparity of methods is that each approach has

notable advantages and limitations in ease of implementation, reproducibility, and correlation to application performance.

BMI applications, such as mind-controlled assistive devices, are driven by information decoded from neural activity, and thus their performance depends on the capacity of the microelectrodes to deliver information. In the nervous system, information is represented by activities of populations of neurons, with each neuron playing a partial and somewhat unique representational role. Multi-electrode implants provide channels of access to these populations, with each electrode recording electrical activity from a few immediately adjacent neurons. An effective microelectrode array should access a sufficient neuronal population to allow distinguishing representations of different thoughts or movements (Li 2014). As well, the device should ensure consistent connectivity to the same neurons at each channel, as the decoding of neural activity relies on custom decoding functions, which are built by characterising how each channel, or neuron, in some decoding schemes, uniquely contributes to the represented information of interest (Green and Kalaska 2011; Wallisch 2014). Consequently, regardless of physical electrode attributes (e.g. impedance, signal-noise-ratio), if the neurons recorded are changing over time, decoding will be miscalibrated and application performance impaired. Although decoding from larger neuronal ensembles can improve reliability (Nuyujukian et al. 2014), optimally engaging a BMI will likely require active neural adaptation (Shenoy and Carmena 2014), which relies on consistently recorded neurons (Ganguly and Carmena 2009b).

The existing metric to address consistency in recorded neurons is to count “stable units”, accomplished via spike-sorting and related techniques (Williams, Rennaker, and Kipke 1999; Liu et al. 1999; Dickey et al. 2009). As multiple neurons fall within an electrode’s recording vicinity, spike-sorting distinguishes the action potentials (spikes) of individual neurons by

grouping each spike according to its waveform. The basis is that an individual neuron's waveform (termed "single unit") is unique due to cell morphology, position with respect to the electrode, and heterogeneity of extracellular composition. Any single unit persisting from previous sessions – matched in attributes that include waveform and inter-spike-interval distribution, is scored as a stable unit. In practice however, due to noise and concurrent neural activity, counting stable units is labour intensive and prone to subjective bias: spike-sorting typically requires human supervision/intervention for every session for every channel, where each result will vary across different software and experts (Harris et al. 2000; Einevoll et al. 2012). While recent developments offer unsupervised alternatives (Takekawa, Isomura, and Fukai 2010; Eleryan et al. 2014), it remains problematic that waveform properties of a neuron fluctuate rapidly (Linderman et al. 2006). Furthermore, identifying stable units by waveform precludes against stable neurons undergoing changes in morphology, position, or local environment – a likely scenario at the site of a foreign body response in reaction to an implanted electrode (Linderman et al. 2006; Kozai et al. 2015). The accuracy of stable unit identification can be improved by examining the response of each single unit to a stimulus or behavior, but such experimental protocols are much more involved than a general recording of neural activity (McMahon et al. 2014; Liu et al. 2006). The stable unit count is also more exigent than necessary to predict application performance, as newer BMI implementations directly decode from channel activity (i.e. using all above-threshold spikes) rather than from sorted single units (Gilja et al. 2012; Fraser et al. 2009; Hochberg et al. 2012).

We present here a novel data analysis technique, the Firing Profile Test (FPT), that specifically tests whether each channel is recording the same group of neurons over time. We aimed to create a stability assessment method that is fast, reproducible, and effective for

predicting application performance. This technique focuses on channel level stability without isolating individual neurons, comparing spike rate statistics between sessions to detect instances of instability (i.e. the loss, addition, or change of neurons at a microelectrode site). FPT is automated and available as MATLAB functions. It is applicable to any dataset where each recording session utilized the same protocol and engaged the probed neural population with an adequate variety of stimulus conditions.

Table 1: Summary of currently employed methods of microelectrode stability evaluation

Metric	Quantity targeted	Minimum requirements	Correlation to decoding reliability, Ease of implementation, Reproducibility
Impedance (Barrese et al. 2013; Prasad et al. 2014; Rousche and Normann 1998; Malaga et al. 2015)	Electrical conductivity and phase shift	- Impedance instrumentation - Any intervention that affects electrode surface	Low, High, Moderate
Amplitude (Malaga et al. 2015; Chestek et al. 2011) or **SNR** (Barrese et al. 2013; Prasad et al. 2014; Suner et al. 2005)	Amplitude of target signal or its ratio to noise floor	- Electrophysiology instrumentation - Live culture/tissue that generate bio electricity	Low, High, High
Above-threshold events (Barrese et al. 2013; Wang et al. 2014)	Large amplitude spikes (single units and multi units)	- Electrophysiology instrumentation - Short term in-vivo implant experiment	Moderate, Moderate, High
Single units (Prasad et al. 2014; Rousche and Normann 1998; Suner et al. 2005; Wang et al. 2014)	Spikes originating from discernible single neurons	- Electrophysiology instrumentation - Short term in-vivo implant experiment - Spike sorting	Moderate, Low, Moderate
Stable units (Vaidya et al. 2014; Eleryan et al. 2014)	Single units that persisted over multiple sessions	- Electrophysiology instrumentation - Short term in-vivo implant experiment - Spike sorting - Stable unit analysis	High, Low, Low
Stable units supported by representation (McMahon et al. 2014; Liu et al. 2006)	Stable units that are consistent to specific stimuli or behaviors	- Multi-channel electrophysiology instrumentation - Short term in-vivo implant experiment - Stimulus-response or behavioral protocol - Spike sorting - Stable unit representation analysis	Very High, Very Low, High
BMI performance (Nuyujukian et al. 2014; Perge et al. 2013)	Performance / throughput on neuro-prosthetic systems	- Multi-channel electrophysiology instrumentation - BMI application system/simulation - Long term in-vivo implant experiment - Behavioral training - Decoder building - Performance/throughput analysis	Very High, Very Low, High
FPT (proposed method)	Distribution of spike-rates under assorted stimuli	- Electrophysiology instrumentation - Short term in-vivo implant experiment - Consistent stimulation or behavioral sequence	High, Moderate, High

4.4 Results

A key obstacle to traditional neuron tracking methods, which rely on analysis of action potential waveforms, is that waveforms are noisy and change over time in stable neurons. The approach we describe here works directly with firing rates, which only require thresholding the analog signal to extract neural population information. Typically, firing rates have significant variability and cannot easily be used to identify neurons. Rather than interpreting firing rates discretely, our method constructs a higher level signature of neural firing capability via a variety of stimuli. Then, relationships between the signatures and neural tuning curves are identified and leveraged to deduce whether a detected change in a signature reflects instability (Figure 1).

4.4.1 Description of method

4.4.1.1 Data input

The input data is the raw recording, organized by channel number and recording session, and the timestamps corresponding to stimulus onset. Datasets that have been converted to spike rasters can be directly used as input data.

For FPT to be effective, the recording experiment should satisfy the following criteria:

1) The recording protocol engages the probed neural population with an adequate variety of test conditions, e.g. on the order of a hundred different images for a visual cortex implant, or movement targets for a motor cortex implant. The ideal range and selection of conditions should be sufficiently wide that each neuron encounters some within and some outside of its criteria for firing, as well as sufficiently nuanced that

each neuron will be activated differently than its neighbouring neurons for some conditions.

2) Each condition should be held for an adequate time window to capture a neuron's spike rate (e.g. if the slowest spike rate of interest is 2 Hz, each condition should be maintained for at least 0.5 s).
3) In each experimental session, recordings should be made using the same protocol (sequence of conditions).

4.4.1.2 Spike raster extraction

If the input data are raw recordings, the software tool first performs a conventional spike raster extraction by filtering and thresholding the signal. Users can configure the default settings or replace this step with a custom module. Typically, the threshold level is selected such that spikes exceeding this amplitude are single-units or distinct multi-units. Outputs from this step are the timestamps of above-threshold spikes. Spike waveforms are not relevant to FPT.

4.4.1.3 Descriptive statistics and channel stability visualization

FPT focuses on spike rate statistics at the channel level, where the output of one channel is the superimposition of multiple neurons within its recording range. For brevity, these neurons will be termed the "channel-population". The descriptive statistic of interest, i.e. the high-level firing signature, is the spike-rate-histogram of each channel-population from each recording session. Spike-rate-histograms are generated automatically from spike raster data by the software tool, by performing the following: 1) divide the data into epochs by test condition onset, 2) count spikes (averaging repetitions of the same condition), and convert to spike-rate (Hz) per

condition, 3) plot histograms of the tabulated spike rates, akin to a frequency domain distribution, that includes all test conditions. Thus, a histogram displays the number of occurrences of each spike rate, where each occurrence reflects one test condition.

Intuitively, the spike-rate-histogram illustrates a channel-population's firing capability. The shape of the distribution shows the population's tendency or preference to fire at each frequency, and the area under the distribution represents how many test conditions, in total, had induced spiking activity. The spike-rate-histogram is suitably sensitive for visualizing stability when different sessions are compared, as it does not discern the specific neural activity per condition, which would exhibit significant trial to trial variability (Azouz and Gray 1999), yet it is perturbed by differences in the channel-population's characteristic output levels and size of its representation domain (i.e. receptive field or behavioral target). The software tool outputs a collection of histograms and displays them as a heatmap to allow users to directly inspect each channel's stability profile (Figure 1, panel III).

4.4.1.4 Stability detection and summary of implant performance

Next, FPT formally tests for instability by inspecting the salient features of each spike-rate-histogram, according to its relationship to the neural tuning curve. This method is designed to assess the consistency of channel-populations over time, thus, instability is defined as the addition, loss, or replacement of neurons. The current version of FPT uses a rule-based reasoning (RBR) function to compare each spike-rate-histogram with that of the previous session to discern instances of population change (unstable) vs. natural modulations (stable).

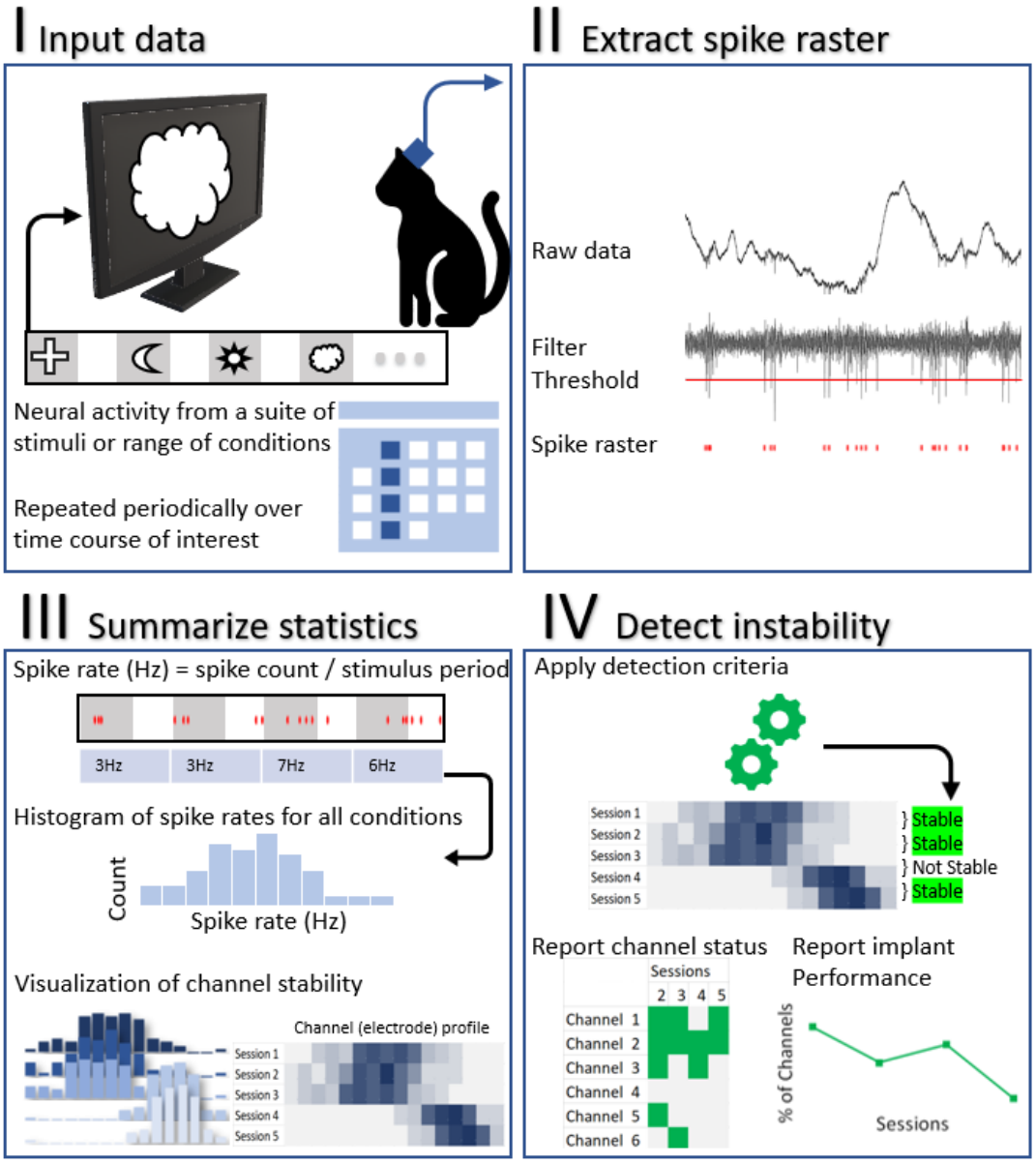

Figure 1: Workflow of the Firing-Profile-Test for microelectrode stability assessment

The RBR logic relies on the following facts and assumptions (Figure 2):

1) Features of the spike-rate-histogram describe attributes of the neural tuning curve (Figure 2A), which is a unique property that distinguishes individual neurons.
2) A channel-population's combined tuning curve is the linear combination of its constituent's individual tuning curves.
3) Natural modulations that alter neural firing rates manifest as a contained shift in tuning curve height and x-intercept, while the addition/loss/replacement of neurons alters the combined tuning curve drastically (Figure 2B).

The rules that govern the RBR are listed below. Derivations and a larger set of logic to estimate the cause of recording instability (i.e. added/dropped/changed units) are detailed in the Methods section. Default parameters, derived from the literature (Kayser et al. 2015; Connor et al. 1996; Anton-Erxleben, Stephan, and Treue 2009; Singh et al. 2014), are included in the software tool, and should be customised where possible according to the specific use-case and the characteristics of neurons in the implanted area. Instability has occurred if there is a:

- change in upper or lower bound of the distribution that exceeds anticipated effects of natural modulation
- change in width of the distribution that is bidirectional
- change in area under the distribution that exceeds anticipated effects of natural modulation
- shift in the position of peaks within the distribution

From RBR output, the FPT software tool generates summary charts of the full implant performance, including a map of Channel Status by Session, and a plot of Stability by Time. For these summaries, the software also optionally filters for minimum activity level, such that only stable and sufficiently active channels will be counted.

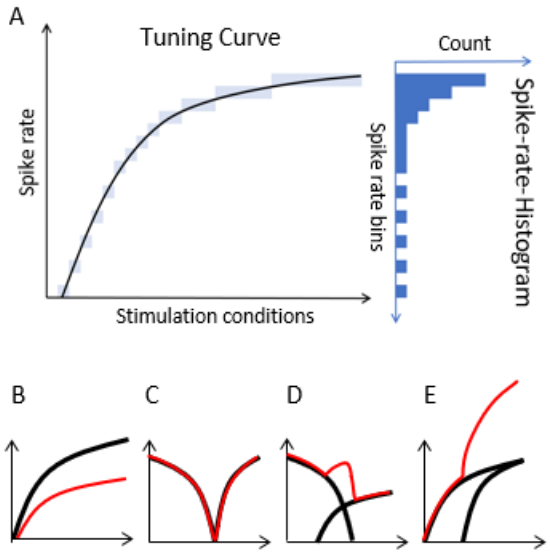

Figure 2: Using the spike-rate-histogram to infer tuning curve changes

A. Relating features of the tuning curve (shown in black) of a hypothetical sensory neuron, to the resulting spike-rate-histogram (shown in blue) when its receptive field is fully stimulated. The highest and lowest histogram bins reflect maximum and minimum curve values, area under the histogram reflects curve length on the x-axis, and histogram peaks reflect ranges with minimum slope. B. How a tuning curve may change due to natural fluctuations, such as attention. C-E. How a tuning curve may change due to the linear combination of two neurons (red is the resulting tuning curve); where C illustrates 2 neurons with non-overlapping curves significantly increasing the resulting receptive field, D illustrates 2 neurons with slightly overlapping curves producing another preferred firing rate, and E illustrates 2 neurons with fully overlapping curves significantly increasing the resulting maximum firing rate.

4.4.2 Performance evaluation by simulation

Simulation has the advantages of creating datasets with known ground truth and unlimited manipulation of experimental parameters, which enables precise evaluation of an algorithm's accuracy and comprehensive testing of its robustness. As FPT only analyzes spike raster data, physical modeling of neurons and analog signal simulation were not required.

A simulated ensemble of "leaky integrate and fire" neurons was generated using Nengo (Eliasmith and Anderson 2003) neural simulator software (Figure 3A). In the ensembles generated, all neurons have the same input dimensions (i.e. number of scalar variables encoded in activity) and physiological parameters but each has a unique tuning curve, characteristic of population encoding. A recording experiment was then simulated within Nengo. The virtual ensemble received a sequence of inputs spanning its representation domain, and each neuron's activity (in spike raster form) was collected.

To simulate channel level instability and automatically test FPT, a self-checking testbench was developed in MATLAB. For each trial, the testbench randomly selects several neurons from the Nengo ensemble as a simulated channel-population and superimposes these neurons' spike rasters to create "recording 1". The testbench then creates "recording 2" by applying a randomly selected testcase: for an unstable testcase, by revising the channel-population (i.e. adding, replacing or removing neurons), and for a stable case, by modulating the same channel-population (i.e. duplicating "recording 1" and manipulating spike rates by a random percentage). Finally, the testbench calls FPT to test the stability between "recording 1" and "recording 2" and determines whether the verdict matches the ground truth (i.e. the selected testcase).

To quantify FPT accuracy, ten sets of one hundred trials were run by the testbench per configuration. For nominal cases, i.e. one or two-dimensional neurons of maximum 200 Hz firing rate, with up to three neurons per channel-population, FPT performed at 90% accuracy (in correctly identifying if a pair of simulated recordings were stable or unstable to each other). To evaluate robustness, testing was repeated with more challenging simulation parameters, including: lower firing rates, larger channel-populations, and reduced coverage of the representation domain. Results from the testbench are summarized in Figure 3B.

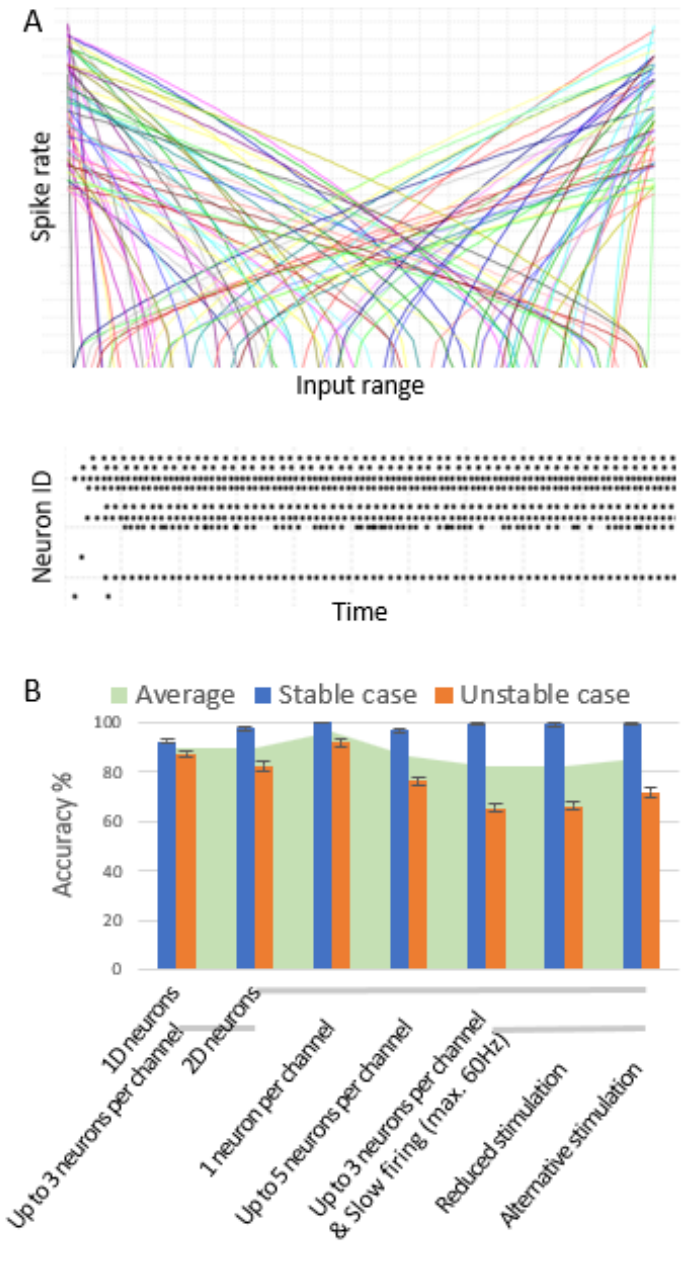

Figure 3: Performance evaluation by simulation

A. Example of a simulated ensemble of neurons with assorted tuning curves, where neural responses are plotted against the range of possible stimuli (e.g. the frequency of a tone for auditory neurons) (top), and an excerpt of simulated spiking activity (bottom) when stimulated with an incrementally increasing input. B. Accuracy of the current version of FPT, evaluated using 10 sets of 100 random test cases per test condition (as labeled below bar plot). Error bars show s.e.m. Note the accuracy for detecting stable cases is higher than unstable cases, thus the final stability estimates will be conservative.

4.4.3 Performance comparison with supervised spike-sorted results

To compare FPT with the alternative approach of supervised spike-sorting and human stable-unit quantification, recordings from a Utah-array implanted in a macaque monkey, where 11 sessions were sorted by human experts using Wave-Clus (Quiroga, Nadasdy, and Ben-Shaul 2006) software, was analysed with the FPT software tool. In the experiment, the baseline dataset recorded at the beginning of each session (see Methods) included adequate stimulus conditions to meet the requirements of FPT. Raw data and the stimulus timing file were fed into the software tool and analyzed automatically. To assess stability using the sorted units, single-units were manually analyzed via inspection of waveform shape and inter-spike-interval plots to find stable-units across sessions. To mitigate human error, both conservative and liberal decisions of unit stability were recorded (see Methods). Results from all approaches are shown in Figure 4. Inspection at the single-unit level showed perfect corroboration between techniques, where every session that failed FPT exhibited identifiable instability in its sorted units (Figure 4A). Counting the number of channels that are stable over time per implant, stability determined by FPT falls between conservative and liberal manual estimates for 7/10 sessions (Figure 4B). Importantly, the criteria applied by FTP to assess stability are consistent and independent of human variability due to differences in human judgement, generating absolutely reproducible and comparable outcomes between different experimental trials and laboratories.

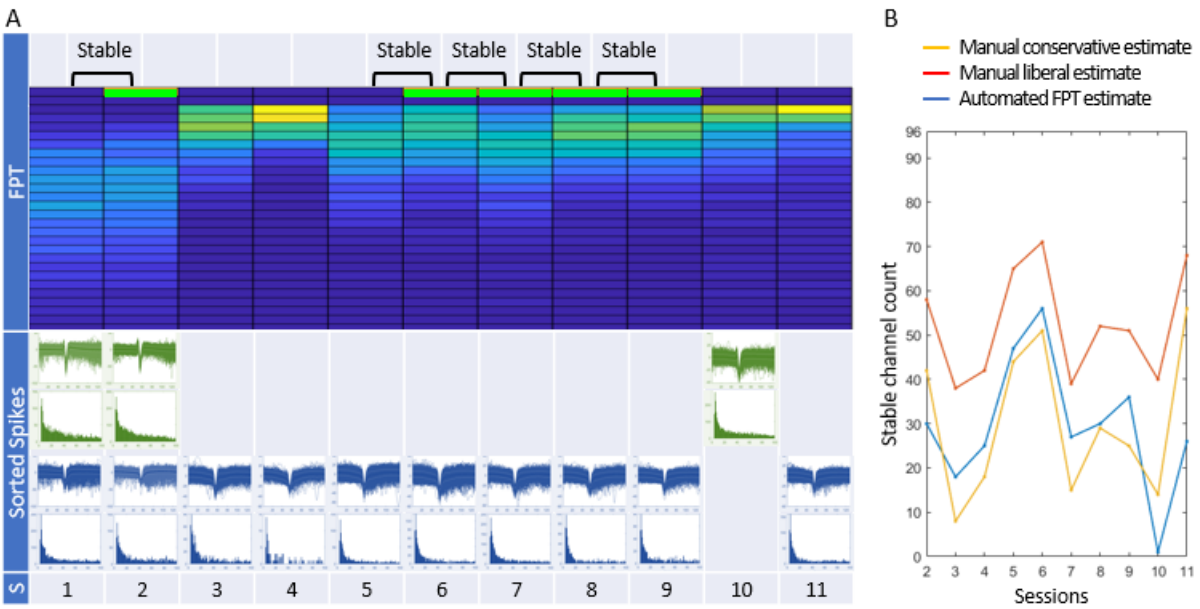

Figure 4: Comparison with stable-units

A. Inspection of sorted units shows that FPT verdicts closely follow instabilities exhibited in single-units: between sessions 2 and 3 (S2-3), one of two units dropped out of recording; between S3-4-5, the remaining unit faded out and back (spike count decrease by ~75%); and between S9-10-11, the two units alternated in their presence in the recording. B. Implant level comparison of the FPT method vs. liberal and conservative manual counting of stable-units. Estimates for stable channel count from FPT falls within the bounds of human counting for 7/10 sessions.

4.4.4 Application to chronically implanted Utah-array dataset

To demonstrate advantages of FPT stability screening, two large datasets from another macaque monkey implanted with two Utah-arrays were analysed, with results illustrated in Figure 5. Such an undertaking would be highly problematic using previously available methods due to requirements on time and human expert labour.

The quantified totals of stable channels are summarized in the Stability by Time plot. Implant 1, an iridium oxide Utah-array located in the left inferotemporal cortex for 8 months duration, provided an average of 8.5 stable channels (out of 96); while implant 2, of the same type and located in the right prefrontal cortex of the same monkey, provided an average of 16 stable channels. The performance of individual channels is illustrated in the Channel Status by Session map, where global failures are easily identifiable as a simultaneous loss of stability across all channels (e.g. sessions 21, 25, 39, 42). Such instances point to implant shift or a system level malfunction. This map also revealed that in spite of activity persisting, implant 1 experienced a catastrophic event 66 days into the recording while implant 2 stability lasted approximately 5 months. The detailed performance of channels of interest are illustrated in the Histogram by Session map (Figure 5). Any active but unstable channel could be examined in this fashion to determine how it introduces variability into the recorded dataset.

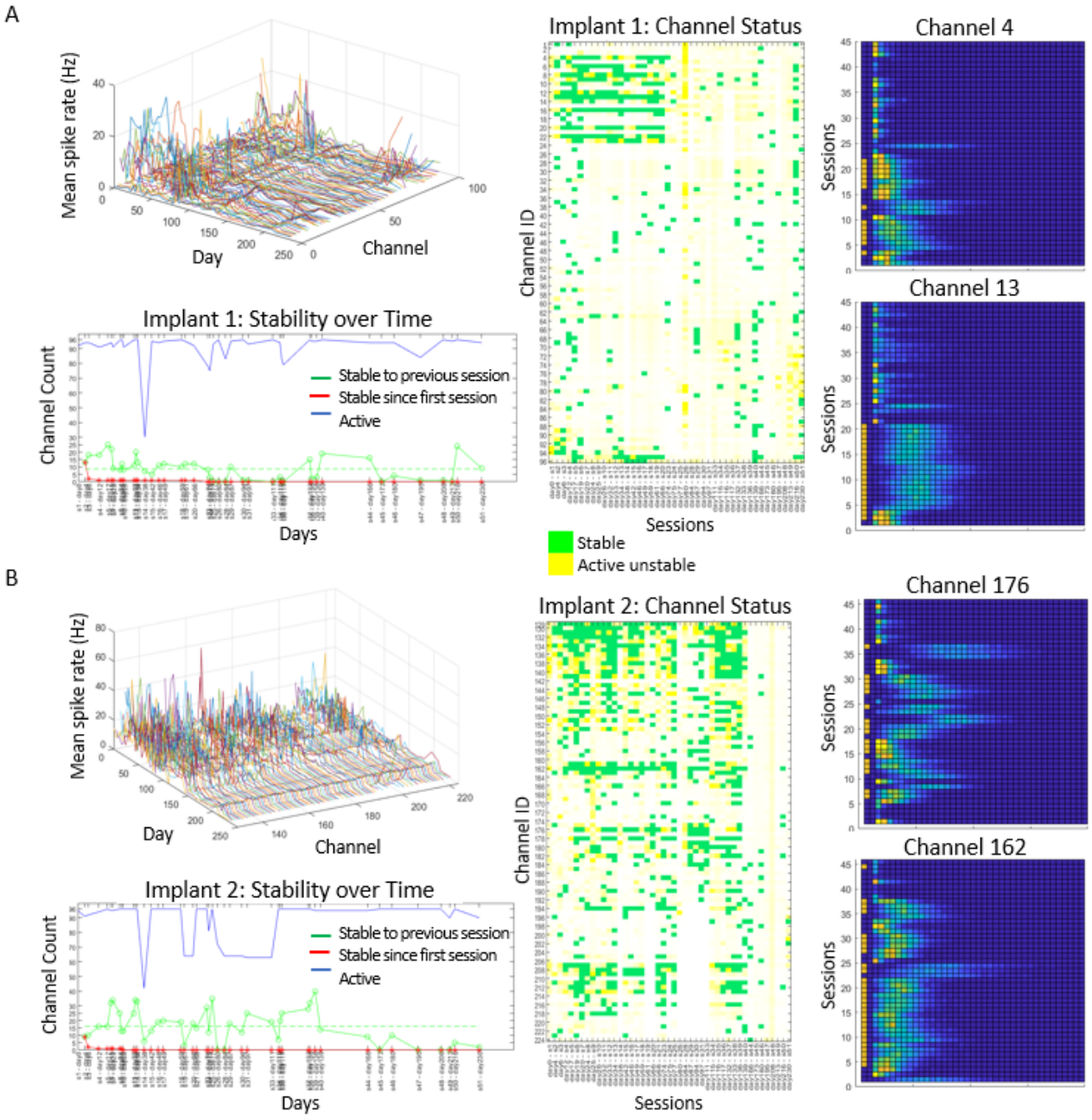

Figure 5: Stability results of two chronically implanted 96-channel Utah-arrays

Datasets from iridium oxide Utah-arrays, implanted in the left inferotemporal (A) and right prefrontal (B) cortices of a macaque monkey over the course of 230 days, were analysed with the FPT method. Plots included are: an overview of mean spike-rates (upper left); Stability over Time (lower left), showing approx. 10-20 channels were stable on average while most channels provided active recordings; Channel Status by Session (middle), showing several channels performed very stably (long green rows) and several sessions encountered global stability failure (long yellow/white columns); as well as Histogram by Session maps (right) for example channels, showing channels 13 & 162 maintained better stability than channels 4 & 176, as their histograms remain vertically aligned over many sessions --provided for reference in the left most bin is FPT's stability verdict for each session.

4.5 Methods

4.5.1 Rule-based reasoning

Rules were developed based on the hypothetical tuning curve of a sensory neuron that encodes for one input variable.

1. Relationship between spike-rate-histogram and tuning curve (Figure 2A):

   If stimulus conditions are selected to uniformly span a neuron's representation domain, each condition within its receptive field will probe a point along the neuron's tuning curve and solicit a response at the encoded spike-rate. Each response will add a single count to the spike-rate histogram, in the corresponding spike-rate bin. Consequently, the number of conditions that fall within the receptive field equals the total number of counts in the spike-rate-histogram, or its area. The neuron's maximum and minimum spike-rates correspond to the highest and lowest filled bins. The shallowest segment of its tuning curve maps to the peak of the histogram (since the largest quantity of conditions evokes this spike-rate).

2. Properties of basic cases of change:

   A neuron undergoing natural modulations (stable case) will have observable changes of the following:

   - Peak spike-rate is modulated by a percentage
   - Receptive field does not change significantly
   - Modulation is congruent over various levels of firing

with equivalent tuning curve changes of (respectively) the following:

- Maximum y-value changes up to a percentage
- X-intercept has minor shifts
- Whole curve scales in consistent direction

The addition of another neuron to the same recording channel (unstable case) will have observable changes of,

- spikes from each neuron superimposed into one stream of activity
- maximum and minimum firing rates redefined by the combined firing pattern
- total receptive field becomes the union of individual receptive fields

with equivalent tuning curve changes of (respectively),

- the combined curve becomes the linear combination of individual tuning curves
- Y-values that summate at each point along the x-axis
- the X-intercept redefined by the combined curve

This case can be further clarified by the following characteristic scenarios:

A. No overlap between receptive fields

- Union of receptive fields
- Maximum spike rate becomes that of the faster neuron, because neurons rarely fire at the same time.

B. Edge overlap between receptive fields

- Union of receptive fields for non-overlapping areas

- Maximum spike rate become that of the faster neuron
- Minimum spike rate increases significantly, because tuning curve has no edge where spike rate drops off

C. Center overlap between receptive fields

- Receptive field becomes that of the broader neuron
- Maximum spike rate increases significantly, because both neurons may fire at maximum rate for the same stimulus

D. Full overlap between receptive fields

- Receptive field does not change
- Maximum spike rate increases significantly, because both neurons may fire at maximum rate for the same stimulus

3. Logical rules:

Detection of instability: test if the differences between two histograms exceed the effects attributable to natural modulation, via the relationship between tuning curves and histograms (Table 2A). Prediction of cause of instability: if instability was detected, check if changes are consistent with gain vs. loss of neurons (Table 2B).

Table 2. Rules for detection of instability (A) and estimation of type of change (B).

A

Rule	Implication
If difference in histogram area > FIELD_THRES	Receptive field size has changed beyond threshold of anticipated modulatory effects
If difference in highest bin position > RATE_THRES	Spike-rate has changed beyond threshold of anticipated modulatory effects
If sign of difference in highest bin position ≠ sign of difference in lowest bin position	Maximum and minimum spike-rates have changed in conflicting directions
If sign of difference in area ≠ sign of difference in highest bin position	Receptive field size has changed in conflicting direction to maximum spike-rate change
If difference in peak position > PEAK_SHIFT_THRES	Preferred spike-rate did not scale proportionally
⇨ Not stable (if any of the above is true)	

B

Rule	Implication
If difference in area > 0 AND difference in highest bin position ≥ 0, OR If difference in highest bin position > 0 AND difference in area ≥ 0, OR If difference in lowest bin position > 0 AND difference in area ≥ 0 AND difference in highest bin position ≥ 0	Receptive field increased while maximum spike-rate did not decrease, OR Maximum spike-rate increased while receptive field did not decrease, OR Minimum spike-rate increased while maximum-spike rate and receptive field did not decrease
⇨ Addition of neurons	
If difference in area < 0 AND difference in highest bin position ≤ 0, OR If difference in highest bin position < 0 AND difference in area ≤ 0, OR If difference in lowest bin position < 0 AND difference in area ≤ 0 AND difference in highest bin position ≤ 0	Receptive field decreased while maximum spike-rate did not increase, OR Maximum spike-rate decreased while receptive field did not increase, OR Minimum spike-rate decreased while maximum-spike rate and receptive field did not increase
⇨ Loss of neurons	
⇨ Change of neurons (if none of the above are true)	

4. Default threshold values

RATE_THRES = 45%, acceptable change in the maximum firing rate (from literature: 45% due to LFP phase (Kayser et al. 2015), 26% due to attention (Connor et al. 1996), 29-85% due to exercise (Singh et al. 2014))

FIELD_THRES = 10%, acceptable change in the range of representation domain, e.g. receptive field size (from literature: 5-14% due to attention (Anton-Erxleben, Stephan, and Treue 2009))

PEAK_SHIFT_THRES = 10%, flexibility for the preferred firing rate to change disproportionally from maximum firing rate

4.5.2 Nengo simulation

The Neural Engineering Framework, Nengo (v1.4.0), was used to simulate ensembles of leaky-integrate-and-fire (LIF) neurons. A Nengo ensemble consists of neurons with the same attributes but assorted tuning curves, which is capable of collectively representing input variables in the manner of population encoding. Thus, neurons within a Nengo ensemble are a fitting approximation for neurons in close proximity to an electrode, as they are likely to have relatively homogenous roles.

Nengo ensembles have input and output terminals that could be connected to form networks. Input terminals could also be driven by function generators that produce a user specified stimulus. While stimulation is applied to the network, ensembles were recorded via virtual probes to collect spike rasters of each neuron in the ensemble (Figure 3A).

Several simulations were created:

1. One-dimensional case (neurons encode for a single variable x):
   - Two ensembles of 100 LIF 1D neurons linked together, each having maximum firing rates between 100-200Hz and radius (representation domain magnitude) of 1.0.
   - Stimulus gradually increases from -1 and 1 using the expression $x = 0.025t - 1$
   - 80 second simulation time – to allow x to reach 1, while collecting spikes from the second ensemble.

2. Two-dimensional case (neurons encode for x & y):
   - Ensemble of 100 LIF 2D neurons with maximum firing rates between 100-200Hz and radius of 1.0.
   - Stimulus draws an ellipse using the expressions $x = 0.5\sin(t)$, $y = \cos(t)$
   - 63 second simulation time – to allow the ellipse to repeat 10 times (each loop requires 2π seconds), while collecting spikes from the ensemble.

3. Slower firing neurons:
   - Same as above with maximum firing rates between 1-30Hz

4.5.3 Testbench

An automated testbench was developed in MATLAB to assess the accuracy of the RBR logic via Nengo simulated datasets. The testbench script, EvalAccuracy, consists of the following elements:

1. Configurations

   For creating test cases

   - Number of cases to generate
   - Limit on size of electrode-population
   - Limit on excitability modulation

   For executing RBR

   - Dataset attributes (specifically for Nengo simulations)
   - Stability and activity thresholds (replicates configurations in the FPT software)

2. Generate test cases and populate with spike-rate-histograms
   - Randomly select neurons from the Nengo simulated ensemble to form an electrode-population.
   - Merge spike rasters of selected neurons and generate spike-rate-histogram 1 (via the Nengo_GenSpikeRateHist function).
   - Randomly select a stability case from list: STABLE, ADD_NEURONS, LOSE_NEURONS, SWITCH_NEURONS.
   - If selected case is not STABLE, modify the current electrode-population by adding, removing, or replacing a random number of neurons – using other randomly selected neurons from the simulated ensemble.
   - Randomly select a modulation amount.
   - Merge spike rasters of the revised electrode-population, apply modulation, and generate spike-rate-histogram 2 (via the Nengo_GenSpikeRateHist_modExcitability function).
   - Repeat above to generate the required number of test cases

3. Run RBR module and collect test results
    - For each test case call the RBR logic (TestStability function).
    - Save all RBR outputs along with the ground truth (the selected cases in step 2).

4. Report accuracy
    - Check RBR results against ground truth
    - Tabulate and display accuracy for stable vs. unstable cases, and details on RBR performance (false positives, false negatives, and error rate of each detection rule).

4.5.4 FPT evaluation via custom testbench and Nengo simulation

The custom testbench was used to test FPT under various configurations, detailed below. (Note each configuration is incremental, the unspecified parameters are the same as the previous configuration).

Configuration 1:

Neuron model = LIF
Dimension (number of scalar variables encoded) = 1
Ensemble size = 100 (2 ensembles)
Maximum firing rate = 100 – 200Hz
Radius (representation domain) = 1.0
Function generator expression = x = 0.025t -1
Simulation (recording) duration = 80s

Number of test cases = 100
Maximum electrode-population size = 3
Maximum modulation = 40%

RATE_THRES = 40%
FIELD_THRES = 10%
PEAK_SHIFT_THRES =10%

Configuration 2:

Dimension = 2
Function generator expression = x = 0.5sin(t), y = cos(t)
Simulation duration = 63s

Configuration 3:

Maximum electrode-population size = 1

Configuration 4:

Maximum electrode-population size = 5

Configuration 5:

Maximum electrode-population size = 3
Maximum firing rate = 1 – 30Hz

Configuration 6:

Function generator expression = x = 0.4sin(t), y = 0.8cos(t)

Configuration 7:

Function generator expression = x = sin(t), y = 0.5cos(t)

4.5.5 Analysis of Utah-array data and stable-unit quantification

Existing datasets from long-term visual system studies of macaque monkeys were analyzed with FPT. In these experiments, iridium oxide Utah-arrays were implanted in the left inferotemporal and right prefrontal cortices of monkey M and monkey F. MEA output was collected at 30Khz. Before each experiment an 8-minute baseline was recorded using the same fixation point and series of visual stimuli (10 repetitions of 100 natural images per session). The baseline recordings were used for FPT stability analysis. Some sessions recorded from Monkey

M were previously spike-sorted by human experts using Wave-Clus (Quiroga, Nadasdy, and Ben-Shaul 2006) software.

The spike sorted sessions from monkey M were manually analyzed for stable-units. For each channel for each session, the waveform and ISI distribution of each single-unit was visually compared to that of single-units in the previous session. Observations were recorded as three tallies: count of single-units, conservative count of stable-units, and liberal count of stable-units. If both (waveform and ISI) attributes appeared to match for a unit, it was counted as a stable-unit; if only one attribute matched while the other is ambiguous, it was still counted in the liberal tally but excluded from the conservative tally. This is to compensate for bias against neurons that may have changed in morphology or local environment (impacting its waveform) and errors in the original spike-sorting (impacting its ISI distribution).

FPT parameters used:

Raw signal filtering = 250Hz-7.5KHz (Gilja et al. 2012)
Thresholding for spike detection = -4.5RMS (Gilja et al. 2012)
RATE_THRES = 40%
FIELD_THRES = 10%
PEAK_SHIFT_THRES = 10%

4.6 Discussion

We have developed a data analysis method, the Firing-Profile-Test implemented in MATLAB, that automatically analyzes large electrophysiology datasets, screens active implants for electrode stability, and provides detailed channel profiles over the recording history. Comprehensive stability assessment with the speed and objectivity that we demonstrate here was previously unattainable.

Previous approaches to assess neural interface stability track neurons by sorting the analog waveform of action potentials. Here we show that it is possible and advantageous to track neuronal populations using only the time of occurrence of action potentials (i.e. the spike raster). More specifically, FPT identifies changes in the distribution of action potential firing-rate under varied stimuli, as a signature of firing capability, to determine shifts in neuronal tuning curves. Vast improvement in speed and reproducibility arise from two distinctions: 1) FPT consists of simple operations that are ideally suited for automation, while spike-sorting requires input from an experienced user and apt usage of complex computations. 2) FPT analyzes spike rates, congruent with the neural code and BMI decoding, and leverages signal cleanliness afforded by the all or nothing nature of action potentials; while spike-sorting focuses on analog waveform features imparted by physical heterogeneity, which is impacted by many of the noise sources in the biological and recording systems.

We applied FPT to long term recordings from two 96-channel iridium oxide Utah-arrays implanted in the inferotemporal and prefrontal cortices of macaque monkeys. The analysis identified approximately 10-20 stable channels over an eight-month duration for the two implants, punctuated by global stability failures, until a catastrophic occurrence that terminated

stability permanently. As FPT results are absolutely reproducible, these findings can serve as a first stability benchmark of the FDA approved Utah-array for investigators to begin benchmarking alternative neural interfaces. FPT offers an avenue toward standardizing MEA stability assessment. If adopted, such a standard would accelerate progress in the field by providing the means to evaluate new MEA prototypes against other emerging technologies, and give users and system builders the clarity and confidence to adopt novel technologies.

FPT provides clear benefits for neurologists and electrophysiologists that record from MEAs. Active implants can be screened regularly with FPT to monitor interface stability, allowing timely medical attention and troubleshooting, as well as aligning recording sessions to periods of stability, thus saving time and eliminating data holes. Research questions that require consistent neural connectivity, such as in learning and plasticity, becomes accessible with simplified hardware and protocols. Furthermore, existing datasets can be filtered to eliminate confounds caused by instances of instability, or reconsolidated to generate large contiguous datasets to analyze long-term phenomena and train machine learning models.

A powerful potential application of FPT is stability compensation for neural decoders, to promote robustness and reliability of neural interfaces for end users – currently a major roadblock to BMI adoption. As detecting instability is a critical pre-requisite to compensating instability, FPT would facilitate a new paradigm of adaptive decoding. Despite day-to-day alterations in neural function and recording fidelity, the same neurons reside by each electrode site. Therefore, in the simplest implementation, a database of decoders can be created via a training period (e.g. several weeks of implant activity) that encompass various states of each channel, indexed by FPT signatures. Hence during daily use of the neural interface, such a system would regularly assess implant stability with FPT and apply the most optimal decoders;

or if too few stable channels remain, direct the performance of custom calibration for critical channels.

Another roadblock to BMI adoption is the cumbersome hardware required to amplify and transmit neural activity. – Small, fully-implanted wireless solutions are essential for end user safety and convenience. Recent advances in BMI directly decode from spike raster data (Gilja et al. 2012; Fraser et al. 2009; Hochberg et al. 2012), forgoing spike-sorting. FPT complements this approach and directly tracks neuronal populations from spike raster data. This suite of techniques obviates the need for analog signal analysis for BMI operation; paving the way for dramatically miniaturized and lower power devices that only transmit spike raster data.

Accuracy of FPT relies on appropriate thresholds for firing-rate parameters, which will benefit from user customization according to the use-case and the specific neurons that populate the implanted area. A theoretical limitation of FPT is that if a neuron is replaced by another with a very similar tuning curve, the instability will not be detected; however, such instability is also imperceptible to most BMI applications.

FPT provides high-speed reproducible stability assessment of microelectrode-arrays that will facilitate neural interface R&D, enhance the utility of existing interfaces, and enable the development of next generation software and hardware for practical BMI technology.

4.7 References

Anton-Erxleben, Katharina, Valeska M. Stephan, and Stefan Treue. 2009. 'Attention Reshapes Center-Surround Receptive Field Structure in Macaque Cortical Area MT', *Cerebral Cortex*, 19: 2466-78-78.

Azouz, Rony, and Charles M. Gray. 1999. 'Cellular Mechanisms Contributing to Response Variability of Cortical Neurons In Vivo', *Journal of Neuroscience*, 19: 2209-23-23.

Barrese, James C., Naveen Rao, Kaivon Paroo, Corey Triebwasser, Carlos Vargas-Irwin, Lachlan Franquemont, and John P. Donoghue. 2013. 'Failure mode analysis of silicon-based intracortical microelectrode arrays in non-human primates', *Journal of Neural Engineering*, 10: 066014.

Bettinger, Christopher J. 2018. 'Recent advances in materials and flexible electronics for peripheral nerve interfaces', *Bioelectronic Medicine*, 4: 6.

Chestek, Cynthia A., Vikash Gilja, Paul Nuyujukian, Justin D. Foster, Joline M. Fan, Matthew T. Kaufman, Mark M. Churchland, Zuley Rivera-Alvidrez, John P. Cunningham, Stephen I. Ryu, and Krishna V. Shenoy. 2011. 'Long-term stability of neural prosthetic control signals from silicon cortical arrays in rhesus macaque motor cortex', *Journal of Neural Engineering*, 8: 045005.

Connor, Charles E., Jack L. Gallant, Dean C. Preddie, and David C. Van Essen. 1996. 'Responses in Area V4 Depend on the Spatial Relationship Between Stimulus and Attention', *Journal of Neurophysiology*, 75.

Dickey, Adam S., Aaron Suminski, Yali Amit, and Nicholas G. Hatsopoulos. 2009. 'Single-Unit Stability Using Chronically Implanted Multielectrode Arrays', *Journal of Neurophysiology*, 102: 1331-39-39.

Durand, Dominique M., Maysam Ghovanloo, and Elliot Krames. 2014. 'Time to address the problems at the neural interface', *Journal of Neural Engineering*, 11: 020201.

Einevoll, Gaute T., Felix Franke, Espen Hagen, Christophe Pouzat, and Kenneth D. Harris. 2012. 'Towards reliable spike-train recordings from thousands of neurons with multielectrodes', *Current Opinion in Neurobiology*, 22: 11-17-17.

Eleryan, Ahmed, Mukta Vaidya, Joshua Southerland, Islam S. Badreldin, Karthikeyan Balasubramanian, Andrew H. Fagg, Nicholas Hatsopoulos, and Karim Oweiss. 2014. 'Tracking single units in chronic, large scale, neural recordings for brain machine interface applications', *Frontiers in Neuroengineering*, 7: 23.

Eliasmith, Chris, and C. H. Anderson. 2003. *Neural engineering : computation, representation, and dynamics in neurobiological systems* (MIT Press: Cambridge, Mass. ; London).

Fraser, George W., Steven M. Chase, Andrew Whitford, and Andrew B. Schwartz. 2009. 'Control of a brain–computer interface without spike sorting', *Journal of Neural Engineering*, 6: 055004.

Ganguly, Karunesh, and Jose M. Carmena. 2009b. 'Emergence of a Stable Cortical Map for Neuroprosthetic Control', *PLoS Biology*, 7: e1000153.

Gilja, Vikash, Paul Nuyujukian, Cindy A. Chestek, John P. Cunningham, Byron M. Yu, Joline M. Fan, Mark M. Churchland, Matthew T. Kaufman, Jonathan C. Kao, Stephen I. Ryu, and Krishna V. Shenoy. 2012. 'A high-performance neural prosthesis enabled by control algorithm design', *Nature Neuroscience*, 15: 1752.

Green, Andrea M., and John F. Kalaska. 2011. 'Learning to move machines with the mind', *Trends in Neurosciences*, 34: 61-75-75.
Harris, Kenneth D., Darrell A. Henze, Jozsef Csicsvari, Hajime Hirase, and György Buzsáki. 2000. 'Accuracy of Tetrode Spike Separation as Determined by Simultaneous Intracellular and Extracellular Measurements', *Journal of Neurophysiology*, 84: 401-14-14.
Hochberg, Leigh R., Daniel Bacher, Beata Jarosiewicz, Nicolas Y. Masse, John D. Simeral, Joern Vogel, Sami Haddadin, Jie Liu, Sydney S. Cash, Patrick van der Smagt, and John P. Donoghue. 2012. 'Reach and grasp by people with tetraplegia using a neurally controlled robotic arm', *Nature*, 485: 372.
Kayser, Christoph, Caroline Wilson, Houman Safaai, Shuzo Sakata, and Stefano Panzeri. 2015. 'Rhythmic Auditory Cortex Activity at Multiple Timescales Shapes Stimulus–Response Gain and Background Firing', *The Journal of Neuroscience*, 35: 7750-62-62.
Kozai, Takashi D. Y., Andrea S. Jaquins-Gerstl, Alberto L. Vazquez, Adrian C. Michael, and X. Tracy Cui. 2015. 'Brain Tissue Responses to Neural Implants Impact Signal Sensitivity and Intervention Strategies', *ACS Chemical Neuroscience*, 6: 48-67-67.
Li, Zheng. 2014. 'Decoding methods for neural prostheses: where have we reached?', *Frontiers in Systems Neuroscience*, 8: 129.
Linderman, M. D., V. Gilja, G. Santhanam, A. Afshar, S. Ryu, T. H. Meng, and K. V. Shenoy. 2006. 'Neural Recording Stability of Chronic Electrode Arrays in Freely Behaving Primates', *2006 International Conference of the IEEE Engineering in Medicine and Biology Society*: 4387-91-91.
Liu, Xindong, D. B. McCreery, R. R. Carter, L. A. Bullara, T. G. H. Yuen, and W. F. Agnew. 1999. 'Stability of the interface between neural tissue and chronically implanted intracortical microelectrodes', *IEEE Transactions on Rehabilitation Engineering*, 7: 315-26-26.
Liu, Xindong, Douglas B. McCreery, Leo A. Bullara, and William F. Agnew. 2006. 'Evaluation of the Stability of Intracortical Microelectrode Arrays', *IEEE Transactions on Neural Systems and Rehabilitation Engineering*, 14: 91-100-00.
Malaga, Karlo A., Karen E. Schroeder, Paras R. Patel, Zachary T. Irwin, David E. Thompson, J. Nicole Bentley, Scott F. Lempka, Cynthia A. Chestek, and Parag G. Patil. 2015. 'Data-driven model comparing the effects of glial scarring and interface interactions on chronic neural recordings in non-human primates', *Journal of Neural Engineering*, 13: 016010.
McMahon, David B. T., Igor V. Bondar, Olusoji A. T. Afuwape, David C. Ide, and David A. Leopold. 2014. 'One month in the life of a neuron: longitudinal single-unit electrophysiology in the monkey visual system', *Journal of Neurophysiology*, 112: 1748-62-62.
Normann, Richard A., and Eduardo Fernandez. 2016. 'Clinical applications of penetrating neural interfaces and Utah Electrode Array technologies', *Journal of Neural Engineering*, 13: 061003.
Nuyujukian, Paul, Jonathan C. Kao, Joline M. Fan, Sergey D. Stavisky, Stephen I. Ryu, and Krishna V. Shenoy. 2014. 'Performance sustaining intracortical neural prostheses', *Journal of Neural Engineering*, 11: 066003.
Perge, János A., Mark L. Homer, Wasim Q. Malik, Sydney Cash, Emad Eskandar, Gerhard Friehs, John P. Donoghue, and Leigh R. Hochberg. 2013. 'Intra-day signal instabilities

affect decoding performance in an intracortical neural interface system', *Journal of Neural Engineering*, 10: 036004.
Prasad, Abhishek, Qing-Shan Xue, Robert Dieme, Viswanath Sankar, Roxanne C. Mayrand, Toshikazu Nishida, Wolfgang J. Streit, and Justin C. Sanchez. 2014. 'Abiotic-biotic characterization of Pt/Ir microelectrode arrays in chronic implants', *Frontiers in Neuroengineering*, 7: 2.
Quiroga, R. Quian, Z. Nadasdy, and Y. Ben-Shaul. 2006. 'Unsupervised Spike Detection and Sorting with Wavelets and Superparamagnetic Clustering', *Neural Computation*, 16: 1661-87-87.
Rivnay, Jonathan, Huiliang Wang, Lief Fenno, Karl Deisseroth, and George G. Malliaras. 2017. 'Next-generation probes, particles, and proteins for neural interfacing', *Science Advances*, 3: e1601649.
Rousche, Patrick J., and Richard A. Normann. 1998. 'Chronic recording capability of the Utah Intracortical Electrode Array in cat sensory cortex', *Journal of Neuroscience Methods*, 82: 1-15-15.
Salatino, Joseph W., Kip A. Ludwig, Takashi D. Y. Kozai, and Erin K. Purcell. 2017. 'Glial responses to implanted electrodes in the brain', *Nature Biomedical Engineering*, 1: 862-77-77.
Shenoy, Krishna V, and Jose M Carmena. 2014. 'Combining Decoder Design and Neural Adaptation in Brain-Machine Interfaces', *Neuron*, 84: 665-80-80.
Singh, Amaya M., Robin E. Duncan, Jason L. Neva, and W. Richard Staines. 2014. 'Aerobic exercise modulates intracortical inhibition and facilitation in a nonexercised upper limb muscle', *BMC Sports Science, Medicine and Rehabilitation*, 6: 23.
Suner, Selim, Matthew R. Fellows, Carlos Vargas-Irwin, Gordon Kenji Nakata, and John P. Donoghue. 2005. 'Reliability of Signals From a Chronically Implanted, Silicon-Based Electrode Array in Non-Human Primate Primary Motor Cortex', *IEEE Transactions on Neural Systems and Rehabilitation Engineering*, 13: 524-41-41.
Takekawa, Takashi, Yoshikazu Isomura, and Tomoki Fukai. 2010. 'Accurate spike sorting for multi‐unit recordings', *European Journal of Neuroscience*, 31: 263-72-72.
Vaidya, Mukta, Adam Dickey, Matthew D. Best, Josh Coles, Karthikeyan Balasubramanian, Aaron J. Suminski, and Nicholas G. Hatsopoulos. 2014. 'Ultra-long term stability of single units using chronically implanted multielectrode arrays', *Conference proceedings : ... Annual International Conference of the IEEE Engineering in Medicine and Biology Society. IEEE Engineering in Medicine and Biology Society. Annual Conference*, 2014: 4872-75-75.
Wallisch, Pascal. 2014. *MATLAB for neuroscientists : an introduction to scientific computing in MATLAB* (Elsevier, Academic Press: Amsterdam).
Wang, Dong, Qiaosheng Zhang, Yue Li, Yiwen Wang, Junming Zhu, Shaomin Zhang, and Xiaoxiang Zheng. 2014. 'Corrigendum: Long-term decoding stability of local field potentials from silicon arrays in primate motor cortex during a 2D center out task (2014 J. Neural Eng. 11 036009)', *Journal of Neural Engineering*, 11: 049501.
Williams, Justin C., Robert L. Rennaker, and Daryl R. Kipke. 1999. 'Stability of chronic multichannel neural recordings: Implications for a long-term neural interface', *Neurocomputing*, 26: 1069-76-76.

Chapter 5 – Discussion and conclusions

5.1 General Discussions

Seamless connectivity with the nervous system is almost an insurmountable goal due to the extensive incompatibility between neural and electronic systems. Yet, the pursuit of an effective bridge is both clinically significant, and in some ways, a natural progression of electronic technology –many of which serve to augment ourselves and our experiences in the first place. Perhaps benefiting from ideological motivation, tremendous progress has been made in spite of the challenges, to develop better neural interfaces, understand causes of device failure, and make the best use of existing interface technology.

There would likely not be one perfect BMI for all applications, nor one key feature that "solves" the interface problem. Rather, the multiple aspects presented by the overall challenge will require sophisticated solutions, combined into a concerted interface platform. NeuraLink is an example of such a platform (Musk 2019): the soft, thread-like probes aim to minimize chronic scaring; the surgical robotics fitted with cameras and image recognition ability are designed to minimize blood vessel damage, and be able to efficiently implant a large number of probes over a greater cortical area; and the low-power, high-density proprietary electronics, which allows the system to be fully implanted and wireless, have the goal of minimizing/eliminating risks of infection and connector breakage.

At the same time, all encompassing systems are built upon incremental research results that elucidate specific problems and strategies. The studies described in this thesis aimed to advance three specific areas in the BMI literature.

In the first study, we devised a method for attaching conductive micro-pillars onto an existing substrate, and cultured cortical neurons on a coverslip modified with the features. We observed that both the amounts of synaptophysin and PSD95 (indicative of pre-synaptic and post-synaptic specializations, respectively) are significantly increased around the micro-pillars. As synapses are sites of strong adhesion, the result suggests this method is an effective strategy to boost the physical connectivity between neurons and electrodes.

In the second study, we performed EIS on an *in vitro* MEA, and investigated impedance spectra changes after adsorbing protein and culturing astrocytes on the MEA. The EIS data indicated that neither of the experimentally induced surface changes affected electrode impedance at 1Khz. This suggests that biofouling and minor glial ensheathment is acceptable on an electrode and can be a low priority design consideration. This result also has implications for interpreting *in vivo* impedance data, which is often reported at 1Khz -- if surface changes are invisible at this frequency, then the impedance increase typically observed post-implantation should primarily reflect gliosis progression beyond the electrode surface. Other contributions of this study include a circuit representation of extracellular recording that reconciles the role of impedance, and recommendations on more sensitive frequencies for impedance monitoring.

In the third study, we identified a relationship between the spike-rate-histogram and the tuning curve of neurons when exposed to a suite of stimulation conditions. Several metrics of the spike-rate-histogram were found to be effective indicators of tuning curve changes that are associated with neuron population change at an electrode site. This is a useful alternative to waveform based methods to detect neuron population change because it can be reliably automated. A software tool was developed, which gives the neural interface community an avenue for more standardized stability testing.

5.2 Conclusions and summary

Brain-machine-interfaces (BMIs), more broadly, neural interfaces, is a challenging frontier in biomedical engineering due to extensive differences between the nervous system and electronic systems. Despite these challenges, BMIs may be the most direct avenue to compensate certain disorders of the nervous system. We have made progress in three aspects: 1) a technique for improving electrode connectivity to neurons via microstructures that are designed to induce synaptogenesis; 2) findings to help prioritize electrode design considerations, clarify the role of impedance, and facilitate impedance monitoring; and 3) an automated method for rapid and reproducible evaluation of electrode stability using spike-rate statistics. Together the findings presented in this thesis aim to facilitate the development of enhanced BMIs.

References

Anton-Erxleben, Katharina, Valeska M. Stephan, and Stefan Treue. 2009. 'Attention Reshapes Center-Surround Receptive Field Structure in Macaque Cortical Area MT', *Cerebral Cortex*, 19: 2466-78-78.

Armstrong, Regina C. 1998. 'Isolation and Characterization of Immature Oligodendrocyte Lineage Cells', *Methods*, 16: 282-92.

Azouz, Rony, and Charles M. Gray. 1999. 'Cellular Mechanisms Contributing to Response Variability of Cortical Neurons In Vivo', *Journal of Neuroscience*, 19: 2209-23-23.

Banker, Gary, and Kimberly Goslin. 1998. *Culturing nerve cells* (MIT Press: Cambridge, Mass.).

Barrese, James C., Naveen Rao, Kaivon Paroo, Corey Triebwasser, Carlos Vargas-Irwin, Lachlan Franquemont, and John P. Donoghue. 2013. 'Failure mode analysis of silicon-based intracortical microelectrode arrays in non-human primates', *Journal of Neural Engineering*, 10: 066014.

Bettinger, Christopher J. 2018. 'Recent advances in materials and flexible electronics for peripheral nerve interfaces', *Bioelectronic Medicine*, 4: 6.

Blum, Richard A. 2007. "An Electronic System for Extracellular Neural Stimulation and Recording." In. Atlanta: Georgia Institute of Technology.

Burry, Richard W. 1980. 'Formation of apparent presynaptic elements in response to poly-basic compounds', *Brain Research*, 184: 85-98.

Burry, Richard W. 1982. 'Development of apparent presynaptic elements formed in response to polylysine coated surfaces', *Brain Research*, 247: 1-16.

Carmena, Jose M., Mikhail A. Lebedev, Craig S. Henriquez, and Miguel A. L. Nicolelis. 2005. 'Stable Ensemble Performance with Single-Neuron Variability during Reaching Movements in Primates', *The Journal of Neuroscience*, 25: 10712-16.

Chestek, Cynthia A., Vikash Gilja, Paul Nuyujukian, Justin D. Foster, Joline M. Fan, Matthew T. Kaufman, Mark M. Churchland, Zuley Rivera-Alvidrez, John P. Cunningham, Stephen I. Ryu, and Krishna V. Shenoy. 2011. 'Long-term stability of neural prosthetic control signals from silicon cortical arrays in rhesus macaque motor cortex', *Journal of Neural Engineering*, 8: 045005.

Chuang, A. 2014. 'Retinal implants: a systematic review', *The British Journal of Ophthalmology*, 98.

Connor, Charles E., Jack L. Gallant, Dean C. Preddie, and David C. Van Essen. 1996. 'Responses in Area V4 Depend on the Spatial Relationship Between Stimulus and Attention', *Journal of Neurophysiology*, 75.

Costantino, S., K. G. Heinze, O. E. Martinez, P. De Koninck, and P. W. Wiseman. 2005. 'Two-photon fluorescent microlithography for live-cell imaging', *Microsc Res Tech*, 68: 272-6.

Dickey, Adam S., Aaron Suminski, Yali Amit, and Nicholas G. Hatsopoulos. 2009. 'Single-Unit Stability Using Chronically Implanted Multielectrode Arrays', *Journal of Neurophysiology*, 102: 1331-39-39.

Durand, Dominique M., Maysam Ghovanloo, and Elliot Krames. 2014. 'Time to address the problems at the neural interface', *Journal of Neural Engineering*, 11: 020201.

Einevoll, Gaute T., Felix Franke, Espen Hagen, Christophe Pouzat, and Kenneth D. Harris. 2012. 'Towards reliable spike-train recordings from thousands of neurons with multielectrodes', *Current Opinion in Neurobiology*, 22: 11-17-17.

Eleryan, Ahmed, Mukta Vaidya, Joshua Southerland, Islam S. Badreldin, Karthikeyan Balasubramanian, Andrew H. Fagg, Nicholas Hatsopoulos, and Karim Oweiss. 2014. 'Tracking single units in chronic, large scale, neural recordings for brain machine interface applications', *Frontiers in Neuroengineering*, 7: 23.

Eliasmith, Chris, and C. H. Anderson. 2003. *Neural engineering : computation, representation, and dynamics in neurobiological systems* (MIT Press: Cambridge, Mass. ; London).

Flint, R D, Z A Wright, M R Scheid, and M W Slutzky. 2013. 'Long term, stable brain machine interface performance using local field potentials and multiunit spikes', *Journal of Neural Engineering*, 10.

Frampton, John P, Mathew R. Hynd, Aytekin Vargun, Badri Roysam, and William G. Shain. 2009. 'An in vitro system for modeling brain reactive responses and changes in neuroprosthetic device impedance', *2009 Annual International Conference of the IEEE Engineering in Medicine and Biology Society*: 7155-58.

Fraser, George W., Steven M. Chase, Andrew Whitford, and Andrew B. Schwartz. 2009. 'Control of a brain–computer interface without spike sorting', *Journal of Neural Engineering*, 6: 055004.

Ganguly, K, and J Carmena. 2009a. 'Emergence of a Stable Cortical Map for Neuroprosthetic Control', *PLoS Biology*, 7.

Ganguly, Karunesh, and Jose M. Carmena. 2009b. 'Emergence of a Stable Cortical Map for Neuroprosthetic Control', *PLoS Biology*, 7: e1000153.

Gilja, Vikash, Paul Nuyujukian, Cindy A. Chestek, John P. Cunningham, Byron M. Yu, Joline M. Fan, Mark M. Churchland, Matthew T. Kaufman, Jonathan C. Kao, Stephen I. Ryu, and Krishna V. Shenoy. 2012. 'A high-performance neural prosthesis enabled by control algorithm design', *Nature Neuroscience*, 15: 1752.

Goldman, Jennifer S., Mohammed A. Ashour, Margaret H. Magdesian, Nicolas X. Tritsch, Stephanie N. Harris, Nicolas Christofi, Raja Chemali, Yaakov E. Stern, Greta Thompson-Steckel, Pavel Gris, Stephen D. Glasgow, Peter Grutter, Jean-Francois Bouchard, Edward S. Ruthazer, David Stellwagen, and Timothy E. Kennedy. 2013. 'Netrin-1 Promotes Excitatory Synaptogenesis between Cortical Neurons by Initiating Synapse Assembly', *The Journal of Neuroscience*, 33: 17278.

Gopalakrishnan, Gopakumar, Peter Thostrup, Isabelle Rouiller, Anna Lisa Lucido, Wiam Belkaïd, David R. Colman, and R. Bruce Lennox. 2010. 'Lipid Bilayer Membrane-Triggered Presynaptic Vesicle Assembly', *ACS Chemical Neuroscience*, 1: 86-94.

Green, Andrea M., and John F. Kalaska. 2011. 'Learning to move machines with the mind', *Trends in Neurosciences*, 34: 61-75-75.

Guiraud, Jeanne, Julien Besle, Laure Arnold, Patrick Boyle, Marie-Hélène Giard, Olivier Bertrand, Arnaud Norena, Eric Truy, and Lionel Collet. 2007. 'Evidence of a Tonotopic Organization of the Auditory Cortex in Cochlear Implant Users', *The Journal of Neuroscience*, 27: 7838.

Harris, Kenneth D., Darrell A. Henze, Jozsef Csicsvari, Hajime Hirase, and György Buzsáki. 2000. 'Accuracy of Tetrode Spike Separation as Determined by Simultaneous Intracellular and Extracellular Measurements', *Journal of Neurophysiology*, 84: 401-14-14.

Hilgenberg, L. G., and M. A. Smith. 2007. 'Preparation of dissociated mouse cortical neuron cultures', *J Vis Exp*: 562.

Hochberg, Leigh R., Daniel Bacher, Beata Jarosiewicz, Nicolas Y. Masse, John D. Simeral, Joern Vogel, Sami Haddadin, Jie Liu, Sydney S. Cash, Patrick van der Smagt, and John P. Donoghue. 2012. 'Reach and grasp by people with tetraplegia using a neurally controlled robotic arm', *Nature*, 485: 372.

Hofmann, U, and J Krüger. 2015. 'The chronic challenge—new vistas on long-term multisite contacts to the central nervous system', *Frontiers in Neuroengineering*, 8.

Hotson, Guy, D P McMullen, M S Fifer, M S Johannes, K D Katyal, M P Para, R Armiger, W S Anderson, N V Thakor, B A Wester, and N E Crone. 2016. 'Individual finger control of a modular prosthetic limb using high-density electrocorticography in a human subject', *Journal of Neural Engineering*, 13.

Jarosiewicz, B. 2015. 'Virtual typing by people with tetraplegia using a self-calibrating intracortical brain-computer interface', *Science Translational Medicine*, 7.

Jonas, J B, A M Schmidt, J A Muller-Bergh, U M Schlotzer-Schrehardt, and G O Naumann. 1992. 'Human optic nerve fiber count and optic disc size', *Investigative Ophthalmology & Visual Science*, 33: 2012-18.

Kabu, S, Y Gao, B K Kwon, and V Labhasetwar. 2015. 'Drug delivery, cell-based therapies, and tissue engineering approaches for spinal cord injury', *Journal of Controlled Release*, 219: 141-54.

Kandel, Eric, James Schwartz, and Thomas Jessell. 2013. *Principles of Neural Science 5th Edition* (McGraw-Hill: New York).

Katz, Bernard. 1966. *Nerve, Muscle, and Synapse* (McGraw-Hill: New York).

Kayser, Christoph, Caroline Wilson, Houman Safaai, Shuzo Sakata, and Stefano Panzeri. 2015. 'Rhythmic Auditory Cortex Activity at Multiple Timescales Shapes Stimulus–Response Gain and Background Firing', *The Journal of Neuroscience*, 35: 7750-62-62.

Kozai, Takashi D. Y., Andrea S. Jaquins-Gerstl, Alberto L. Vazquez, Adrian C. Michael, and X. Tracy Cui. 2015. 'Brain Tissue Responses to Neural Implants Impact Signal Sensitivity and Intervention Strategies', *ACS Chemical Neuroscience*, 6: 48-67-67.

Li, Zheng. 2014. 'Decoding methods for neural prostheses: where have we reached?', *Frontiers in Systems Neuroscience*, 8: 129.

Linderman, M. D., V. Gilja, G. Santhanam, A. Afshar, S. Ryu, T. H. Meng, and K. V. Shenoy. 2006. 'Neural Recording Stability of Chronic Electrode Arrays in Freely Behaving Primates', *2006 International Conference of the IEEE Engineering in Medicine and Biology Society*: 4387-91-91.

Liu, Xindong, D. B. McCreery, R. R. Carter, L. A. Bullara, T. G. H. Yuen, and W. F. Agnew. 1999. 'Stability of the interface between neural tissue and chronically implanted intracortical microelectrodes', *IEEE Transactions on Rehabilitation Engineering*, 7: 315-26-26.

Liu, Xindong, Douglas B. McCreery, Leo A. Bullara, and William F. Agnew. 2006. 'Evaluation of the Stability of Intracortical Microelectrode Arrays', *IEEE Transactions on Neural Systems and Rehabilitation Engineering*, 14: 91-100-00.

Lucido, A. L., F. S. Sanchez, P. Thostrup, A. V. Kwiatkowski, S. Leal-Ortiz, G. Gopalakrishnan, D. Liazoghli, W. Belkaid, R. B. Lennox, P. Grutter, C. C. Garner, and D. R. Colman. 2009. 'Rapid Assembly of Functional Presynaptic Boutons Triggered by Adhesive Contacts', *Journal of Neuroscience*, 29: 12449-66.

Magdesian, Margaret H., G. Monserratt Lopez-Ayon, Megumi Mori, Dominic Boudreau, Alexis Goulet-Hanssens, Ricardo Sanz, Yoichi Miyahara, Christopher J. Barrett, Alyson E.

Fournier, Yves De Koninck, and Peter Grütter. 2016. 'Rapid Mechanically Controlled Rewiring of Neuronal Circuits', *The Journal of Neuroscience*, 36: 979-87.
Malaga, Karlo A., Karen E. Schroeder, Paras R. Patel, Zachary T. Irwin, David E. Thompson, J. Nicole Bentley, Scott F. Lempka, Cynthia A. Chestek, and Parag G. Patil. 2015. 'Data-driven model comparing the effects of glial scarring and interface interactions on chronic neural recordings in non-human primates', *Journal of Neural Engineering*, 13: 016010.
Maruo, Shoji, and Tatsuya Saeki. 2008. 'Femtosecond laser direct writing of metallic microstructures by photoreduction of silver nitrate in a polymer matrix', *Optics Express*, 16: 1174.
McMahon, David B. T., Igor V. Bondar, Olusoji A. T. Afuwape, David C. Ide, and David A. Leopold. 2014. 'One month in the life of a neuron: longitudinal single-unit electrophysiology in the monkey visual system', *Journal of Neurophysiology*, 112: 1748-62-62.
Memberg, W D, K H Polasek, R L Hart, A M Bryden, K L Kilgore, G A Nemunaitis, H A Hoyen, M W Keith, and R F Kirsch. 2014. 'Implanted neuroprosthesis for restoring arm and hand function in people with high level tetraplegia', *Archives of physical medicine and rehabilitation*, 95: 1201-11.
Metz, Rachel. 2020. 'Elon Musk shows off a working brain implant — in pigs', CNN Business. https://www.cnn.com/2020/08/28/tech/elon-musk-neuralink/index.html.
Miller, K J, G Schalk, D Hermes, J G Ojemann, and R P N Rao. 2016. 'Spontaneous Decoding of the Timing and Content of Human Object Perception from Cortical Surface Recordings Reveals Complementary Information in the Event-Related Potential and Broadband Spectral Change', *PLoS Compulational Biology*, 12.
Minev, Ivan, Pavel Musienko, Arthur Hirsch, and Quentin Barraud. 2015. 'Electronic dura mater for long-term multimodal neural interfaces', *Science Research Reports*, 347: 159.
Moshayedi, Pouria, Gilbert Ng, and Jessica Kwok. 2014. 'The relationship between glial cell mechanose nsitivity and foreign body reactions in the central nervous system', *Biomaterials*, 35: 3919-25.
Musk, Elon. 2019. 'An Integrated Brain-Machine Interface Platform With Thousands of Channels', *J Med Internet Res*, 21: e16194.
Neto, Joana P., Pedro Baião, Gonçalo Lopes, João Frazão, Joana Nogueira, Elvira Fortunato, Pedro Barquinha, and Adam R. Kampff. 2018. 'Does Impedance Matter When Recording Spikes With Polytrodes?', *Frontiers in Neuroscience*, 12.
Nilsson, James, and Susan Riedel. 2004. *Electric Circuits* (Prentice Hall: New Jersey).
Normann, Richard A., and Eduardo Fernandez. 2016. 'Clinical applications of penetrating neural interfaces and Utah Electrode Array technologies', *Journal of Neural Engineering*, 13: 061003.
Nuyujukian, Paul, Jonathan C. Kao, Joline M. Fan, Sergey D. Stavisky, Stephen I. Ryu, and Krishna V. Shenoy. 2014. 'Performance sustaining intracortical neural prostheses', *Journal of Neural Engineering*, 11: 066003.
Oxley, T J, N L Opie, S E John, G S Rind, S M Ronayne, T L Wheeler, J W Judy, A J McDonald, A Dornom, T J Lovell, C Steward, D J Garrett, B A Moffat, E H Lui, N Yassi, B C Campbell, Y T Wong, K E Fox, E S Nurse, I E Bennett, S H Bauquier, K A Liyanage, N R van der Nagel, P Perucca, A Ahnood, K P Gill, B Yan, L Churilov, C R French, P M Desmond, M K Horne, L Kiers, S Prawer, S M Davis, A N Burkitt, P J Mitchell, D B Grayden, C N May, and T J O'Brien. 2016. 'Minimally invasive

endovascular stent-electrode array for high-fidelity, chronic recordings of cortical neural activity', *Nature Biotechnology*, 34: 320-27.

Pandarinath, C, V Gilja, C H Blabe, P Nuyujukian, A A Sarma, B L Sorice, E N Eskandar, L R Hochberg, J M Henderson, and K V Shenoy. 2015. 'Neural population dynamics in human motor cortex during movements in people with ALS', *eLife*, 4: e07436.

Park, Sharon. 1988. "The Use of Substitute Materials on Historic Building Exteriors." In.: National Park Service, U.S. Department of the Interior.

Pech-Pacheco, J. L., G. Cristobal, J. Chamorro-Martinez, and J. Fernandez-Valdivia. 2000. "Diatom autofocusing in brightfield microscopy: a comparative study." In *Proceedings 15th International Conference on Pattern Recognition. ICPR-2000*, 314-17 vol.3.

Peng, H. B., D. R. Markey, W. L. Muhlach, and E. D. Pollack. 1987. 'Development of Presynaptic Specializations Induced by Basic Polypeptide-Coated Latex Beads in Spinal-Cord Cultures', *Synapse*, 1: 10-19.

Perge, János A., Mark L. Homer, Wasim Q. Malik, Sydney Cash, Emad Eskandar, Gerhard Friehs, John P. Donoghue, and Leigh R. Hochberg. 2013. 'Intra-day signal instabilities affect decoding performance in an intracortical neural interface system', *Journal of Neural Engineering*, 10: 036004.

Pertuz, Said, Domenec Puig, and Miguel Angel Garcia. 2013. 'Analysis of focus measure operators for shape-from-focus', *Pattern Recognition*, 46: 1415-32.

Pettersen, Klas H., Henrik Linden, Anders M. Dales, and Gaute T. Einevoll. 2012. 'Extracellular spikes and current-source density.' in Romain Brette and Alain Destexhe (eds.), *Handbook of Neural Activity Measurement* (Cambridge University Press).

Prasad, Abhishek, Qing-Shan Xue, Robert Dieme, Viswanath Sankar, Roxanne C. Mayrand, Toshikazu Nishida, Wolfgang J. Streit, and Justin C. Sanchez. 2014. 'Abiotic-biotic characterization of Pt/Ir microelectrode arrays in chronic implants', *Frontiers in Neuroengineering*, 7: 2.

Quiroga, R. Quian, Z. Nadasdy, and Y. Ben-Shaul. 2006. 'Unsupervised Spike Detection and Sorting with Wavelets and Superparamagnetic Clustering', *Neural Computation*, 16: 1661-87-87.

Quiroga, Rodrigo. 2007. "Spike Sorting." In.: Scholarpedia.

Ricoult, Sebastien G, Greta Thompson-Steckel, James P Correia, Timothy E Kennedy, and David Junker. 2013. 'Tuning cell-surface affinity to direct cell specific responses to patterned proteins', *Biomaterials*, 35: 727-36.

Rivnay, Jonathan, Huiliang Wang, Lief Fenno, Karl Deisseroth, and George G. Malliaras. 2017. 'Next-generation probes, particles, and proteins for neural interfacing', *Science Advances*, 3: e1601649.

Rousche, Patrick J., and Richard A. Normann. 1998. 'Chronic recording capability of the Utah Intracortical Electrode Array in cat sensory cortex', *Journal of Neuroscience Methods*, 82: 1-15-15.

Salatino, Joseph W., Kip A. Ludwig, Takashi D. Y. Kozai, and Erin K. Purcell. 2017. 'Glial responses to implanted electrodes in the brain', *Nature Biomedical Engineering*, 1: 862-77-77.

Shaw, Gerry, Silas Morse, Miguel Ararat, and Frank L. Graham. 2002. 'Preferential transformation of human neuronal cells by human adenoviruses and the origin of HEK 293 cells', *FASEB journal : official publication of the Federation of American Societies for Experimental Biology*, 16: 869-71.

Shenoy, Krishna V, and Jose M Carmena. 2014. 'Combining Decoder Design and Neural Adaptation in Brain-Machine Interfaces', *Neuron*, 84: 665-80-80.
Singh, Amaya M., Robin E. Duncan, Jason L. Neva, and W. Richard Staines. 2014. 'Aerobic exercise modulates intracortical inhibition and facilitation in a nonexercised upper limb muscle', *BMC Sports Science, Medicine and Rehabilitation*, 6: 23.
Sommakia, S, J Gaire, J L Rickus, and K J Otto. 2014. 'Resistive and reactive changes to the impedance of intracortical microelectrodes can be mitigated with polyethylene glycol under acute in vitro and in vivo settings', *Frontiers in Neuroengineering*, 7.
Sridharan, Arati, Jessica Nguyen, Jeffrey Capadona, and Jit Muthuswamy. 2015. 'Compliant intracortical implants reduce strains and strain rates in brain tissue in vivo', *Journal of Neural Engineering*, 12: 036002.
Suner, Selim, Matthew R. Fellows, Carlos Vargas-Irwin, Gordon Kenji Nakata, and John P. Donoghue. 2005. 'Reliability of Signals From a Chronically Implanted, Silicon-Based Electrode Array in Non-Human Primate Primary Motor Cortex', *IEEE Transactions on Neural Systems and Rehabilitation Engineering*, 13: 524-41-41.
Takekawa, Takashi, Yoshikazu Isomura, and Tomoki Fukai. 2010. 'Accurate spike sorting for multi-unit recordings', *European Journal of Neuroscience*, 31: 263-72-72.
Vaidya, M, A Dickey, and M Best. 2014. "Ultra-long term stability of single units using chronically implanted multielectrode arrays." In *Engineering in Medicine and Biology Society (EMBC), 36th Annual International Conference of the IEEE*. Chicago.
Vaidya, Mukta, Adam Dickey, Matthew D. Best, Josh Coles, Karthikeyan Balasubramanian, Aaron J. Suminski, and Nicholas G. Hatsopoulos. 2014. 'Ultra-long term stability of single units using chronically implanted multielectrode arrays', *Conference proceedings : ... Annual International Conference of the IEEE Engineering in Medicine and Biology Society. IEEE Engineering in Medicine and Biology Society. Annual Conference*, 2014: 4872-75-75.
Veraart, C, C Raftopoulos, J T Mortimer, J Delbeke, D Pins, G Michaux, A Vanlierde, S Parrini, and M C Wanet-Defalque. 1998. 'Visual sensations produced by optic nerve stimulation using an implanted self-sizing spiral cuff electrode', *Brain Research*, 813: 181-86.
Wallisch, Pascal. 2014. *MATLAB for neuroscientists : an introduction to scientific computing in MATLAB* (Elsevier, Academic Press: Amsterdam).
Wang, Dong, Qiaosheng Zhang, Yue Li, Yiwen Wang, Junming Zhu, Shaomin Zhang, and Xiaoxiang Zheng. 2014. 'Corrigendum: Long-term decoding stability of local field potentials from silicon arrays in primate motor cortex during a 2D center out task (2014 J. Neural Eng. 11 036009)', *Journal of Neural Engineering*, 11: 049501.
Williams, Justin C., Joseph A. Hippensteel, John Dilgen, William Shain, and Daryl R. Kipke. 2007. 'Complex impedance spectroscopy for monitoring tissue responses to inserted neural implants', *Journal of Neural Engineering*, 4: 410.
Williams, Justin C., Robert L. Rennaker, and Daryl R. Kipke. 1999. 'Stability of chronic multichannel neural recordings: Implications for a long-term neural interface', *Neurocomputing*, 26: 1069-76-76.
Xie, C, J Liu, T M Fu, X Dai, W Zhou, and C M Lieber. 2015. 'Three-dimensional macroporous nanoelectronic networks as minimally invasive brain probes', *Nature Materials*, 14: 1286-92.
Xie, X., L. Rieth, L. Williams, S. Negi, R. Bhandari, R. Caldwell, R. Sharma, P. Tathireddy, and F. Solzbacher. 2014. 'Long-term reliability of Al2O3 and Parylene C bilayer encapsulated

Utah electrode array based neural interfaces for chronic implantation', *J Neural Eng*, 11: 026016.
Yang, X., T. Zhou, T. J. Zwang, G. Hong, Y. Zhao, R. D. Viveros, T. M. Fu, T. Gao, and C. M. Lieber. 2019. 'Bioinspired neuron-like electronics', *Nat Mater*, 18: 510-17.